

Detection and Characterization Methods of Exoplanets

FREE

Nuno C. Santos, Institute of Astrophysics and Space Sciences, University of Porto (CAUP) & Department of Physics and Astronomy, University of Porto, Portugal,

Susana C.C. Barros, Institute of Astrophysics and Space Sciences, University of Porto (CAUP), Portugal,

Olivier D.S. Demangeon Institute of Astrophysics and Space Sciences, University of Porto (CAUP) & Department of Physics and Astronomy, University of Porto, Portugal,

and João P. Faria Institute of Astrophysics and Space Sciences, University of Porto (CAUP), Portugal

<https://doi.org/10.1093/acrefore/9780190647926.013.189>

Published online: 27 August 2020

Summary

Is the Solar System unique, or are planets ubiquitous in the universe? The answer to this long-standing question implies the understanding of planet formation, but perhaps more relevant, the observational assessment of the existence of other worlds and their frequency in the galaxy.

The detection of planets orbiting other suns has always been a challenging task. Fortunately, technological progress together with significant development in data reduction and analysis processes allowed astronomers to finally succeed. The methods used so far are mostly based on indirect approaches, able to detect the influence of the planets on the stellar motion (dynamical methods) or the planet's shadow as it crosses the stellar disk (transit method). For a growing number of favorable cases, direct imaging has also been successful. The combination of different methods also allowed probing planet interiors, composition, temperature, atmospheres, and orbital architecture. Overall, one can confidently state that planets are common around solar-type stars, low mass planets being the most frequent among them.

Despite all the progress, the discovery and characterization of temperate Earth-like worlds, similar to the Earth in both mass and composition and thus potential islands of life in the universe, is still a challenging task. Their low amplitude signals are difficult to detect and are often submerged by the *noise* produced by different instrumentation sources and astrophysical processes. However, the dawn of a new generation of ground and space-based instruments and missions is promising a new era in this domain.

Keywords: exoplanets, radial velocities, transits, astrometry, direct imaging, microlensing, atmospheres

Introduction

The discovery and characterization of other Earths—rocky planets with the physical conditions to hold liquid water on their surface—is one of the boldest objectives of astrophysics. The community agrees that rocky planets are very common around solar-type stars (e.g., Bonfils et al., 2013; Borucki et al., 2011; Fressin et al., 2013; Howard et al., 2012; Mayor, Lovis, & Santos, 2014; Mordasini, Alibert, Benz, Klahr, & Henning, 2012; Udry & Santos, 2007), and these results motivate the development of a whole new generation of ground and space based instruments and missions by the main international agencies (e.g., ESA, ESO, NASA). Exoplanet research holds the promise of detecting another world where life may have evolved, building new bridges between different fields in astrophysics (e.g., stellar astrophysics, solar system research) and other areas of knowledge such as geophysics (e.g., Valencia, O’Connell, & Sasselov, 2006) and biology (Kaltenegger & Sasselov, 2011).

With the number and diversity of discovered planets growing at an almost daily basis (see the updated Extrasolar Planets Encyclopaedia <http://www.exoplanet.eu>—Schneider, Dedieu, Le Sidaner, Savalle, & Zolotukhin, 2011), the focus of observational research in exoplanet science is turned toward two main lines: (a) the detection of low mass planets, with the goal of finding an Earth sibling and (b) the detailed characterization of known exoplanets, including their interior structures and atmospheres. These lines of research have already seen their own success. Radial velocity (RV) and transit surveys have found an increasing number of low mass/radius planets orbiting other stars (Borucki et al., 2011; Mayor et al., 2014). The precision of the transit measurements, in combination with mass determinations from RV measurements, also allowed deriving the bulk composition of several of these (Léger et al., 2009; Pepe et al., 2013)—see also review by (Howard, 2013). In some favorable cases, exquisite measurements further allowed detection of both the emitted (infrared—IR) and reflected (optical) light of exoplanets, as well as the presence of specific chemical constituents in their atmospheres (Brogi et al., 2012; Martins et al., 2015; Sing et al., 2016)—see also review by Burrows (2014).

As presented throughout this article, the use of different approaches is key to the success of exoplanet science. Detecting a planet orbiting a distant star is not an easy task, and a long way has thus been covered from the early frustrating efforts using the astrometric methods (e.g., van de Kamp, 1983) until the detection of the first exoplanet orbiting a solar-type star (51 Peg b—Mayor & Queloz, 1995) using Doppler radial velocities. In this context, the present article presents the most relevant planet detection and characterization methods, with a focus on those that promise to find and characterise other Earths in the cosmos. It starts by reviewing the main detection methods, their potential and limitations. The challenges imposed by astrophysical noise will also be presented alongside the main approaches to address them. It further briefly reviews the main results from exoplanet research and the prospects for the next decades.

Main Methods

When identifying which methods have been the most prolific so far, the radial velocity and transit techniques are clearly on top of the list. Additionally to their relevance for planet detection, when combined these two methods allow to derive the mass and radius of the

planets, and thus their mean densities. As a consequence, they are presently the main battle-horses for planet detection and characterization. This review begins with a basic description of these two approaches.

Doppler Spectroscopy

The method behind the detection of the first exoplanet orbiting a solar-type star (Mayor & Queloz, 1995) is the radial-velocity (RV) technique. This method is based on the fact that, following Newton's laws, when a star is orbited by a planet, the gravitational pull from the orbiting companion implies that the former will orbit the centre of mass of the star-planet system. This motion can be observable as a variation in the radial-velocity (the velocity projected on the line-of-sight) of the star as a function of time, allowing the detection of companions to solar-type stars even if one cannot *see* their light directly.

From geometrical principles, and assuming that the orbits are ellipsoidal,¹ it can be shown that such a radial velocity (RV) signal can be modeled through the following equation:

$$RV(\nu)\gamma + K[e \cos \omega + \cos(\omega + \nu(t))] \quad (1)$$

This is usually dubbed a *Keplerian function*, as it denotes the radial-velocity variations caused by a planet in a generic *Keplerian* (and elliptical) orbit around the star. Here, K is the RV semi-amplitude, e the orbital eccentricity, and γ is the constant systemic RV (the velocity of the center of mass of the system, relative to us). The angles ω and $\nu(t)$ denote the longitude of periastron of the orbit of the star and the true anomaly, respectively. The longitude of periastron provides the orientation of the orbit with respect to the line of sight, and is fixed for a given orbit. The true anomaly is the angle that gives the position of the body in the ellipse at any given moment in time (t), with reference to its position at periastron. Note that the true anomaly is a function of time t , eccentricity e , the orbital period P , and the moment of periastron, T . For a thorough definition of these variables and more details see Hilditch (2001).

Equation 1 expresses the expected radial velocity as a function of several variables, but not explicitly as a function of time. The time dependence of the true anomaly ν can be computed as follows. For a given moment in time t , and considering the parameters T and P as defined above, compute the so called mean anomaly, M , by the equation:

$$M = 2\pi(t - T)/P \quad (2)$$

From the derived value of M , one can then compute the eccentric anomaly— m , by solving Kepler's equation:

$$M = E - e \sin(E)$$

Finally, it is possible to compute the true anomaly ν , considering the orbital eccentricity e and the derived value for E using:

$$\tan \nu/2 = \sqrt{\frac{1+e}{1-e}} \tan E/2 \quad (4)$$

Note that Kepler's equation is transcendental and needs to be solved by an iterative process (e.g., using the Newton-Raphson method). A simple scheme to solve it is using a procedure like the following:

$$\begin{aligned} E_0 &= M + e \sin M + \frac{e^2}{2} \sin 2M \\ M_0 &= E_0 - e \sin E_0 \\ E_1 &= E_0 + \frac{M - M_0}{1 - e \cos E_0} \\ M_1 &= E_1 - e \sin E_1 \\ &\quad (\dots) \end{aligned} \quad (5)$$

A few iterations are usually enough to achieve convergence.

In brief, if one manages to fit a given radial velocity time series with equation 1, one will immediately be able to derive the following parameters: P , e , K , γ , T , and ω . In turn, these can be used to derive further information about the planet. Using Newton's laws and Kepler's equations, it can be shown that in the simple case of a two body problem, a star of mass M_1 will periodically wobble around its companion (mass M_2).² A velocity semi-amplitude K_1 is expressed by (e.g., Perryman, 2018):

$$K_1 = \left(\frac{2\pi G}{P} \right)^{1/3} \frac{M_2 \sin i}{(M_1 + M_2)^{2/3}} \frac{\sin i}{\sqrt{1 - e^2}} \quad (6)$$

In this equation, i is the inclination of the orbital axis with respect to the line of sight, G is the gravitational constant, P is the orbital period, and e is the orbital eccentricity. In other words, the semi-amplitude K of the RV variations is directly related with the mass of the companion that induces them, with the only uncertainty being the orbital inclination (through the $\sin i$ term).

One immediate limitation of the RV technique follows from here: using this method, one is only able to measure the projected radial-velocity—that is, the component of the radial-velocity in the direction of the line-of-sight. This implies that one can only estimate the

projected mass of the companion responsible for the observed stellar wobble—its minimum mass ($M_2 \sin i$). Fortunately, it can be shown that, for orbits randomly oriented in space, it is much more likely to have $\sin i$ close to unity (e.g., Jorissen, Mayor, & Udry, 2001).³ This means that the minimum masses obtained are statistically close to the real masses. The unambiguous determination of the true mass is possible, however, only if a value for the orbital inclination is obtained (e.g., through a transit measurement).

Equation (6) also shows that the higher the planet mass and the shorter the orbital period, the stronger will be the RV signal. The RV technique is thus more sensitive to shorter period, more massive planets. This explains why the first discoveries announced the existence of a new class of giant planets orbiting in short period orbits, the so-called “hot-jupiters” (Mayor & Queloz, 1995), even if they are relatively rare (see e.g., Santerne et al., 2016).

Measuring Radial Velocities

From equation (6), one can derive that the semi-amplitude K_1 of a star induced by the presence of a Jupiter-like planet (with a mass of $318 M_{\oplus}$ and an orbital period of ~ 12 yr) is only ~ 13 m/s, while for an Earth-like planet this value decreases to a mere ~ 8 cm/s. These numbers illustrate the challenge of detecting a planet using the radial velocity method.

The RV of the star can be measured from the Doppler shift of its spectral lines (see Fig. 1) using high-resolution spectrographs. Doppler’s equation states that $\frac{\Delta\lambda}{\lambda} = \frac{v}{c}$, where c is the speed of light, λ is the reference wavelength (at zero velocity—typically the wavelength of an absorption spectral line in a reference spectral template), $\Delta\lambda$ is the wavelength shift observed, and v is the radial velocity. The biggest challenge of this technique is that one needs to measure the stellar velocity with very high precision. At optical wavelengths, these small amplitudes translate to values of $\Delta\lambda \sim 10^{-4}$ Å. For comparison, a typical high-resolution spectrograph (with a resolution $R=\lambda/\Delta\lambda = 100000$) is only able to resolve two adjacent wavelengths separated by ~ 0.1 Å.

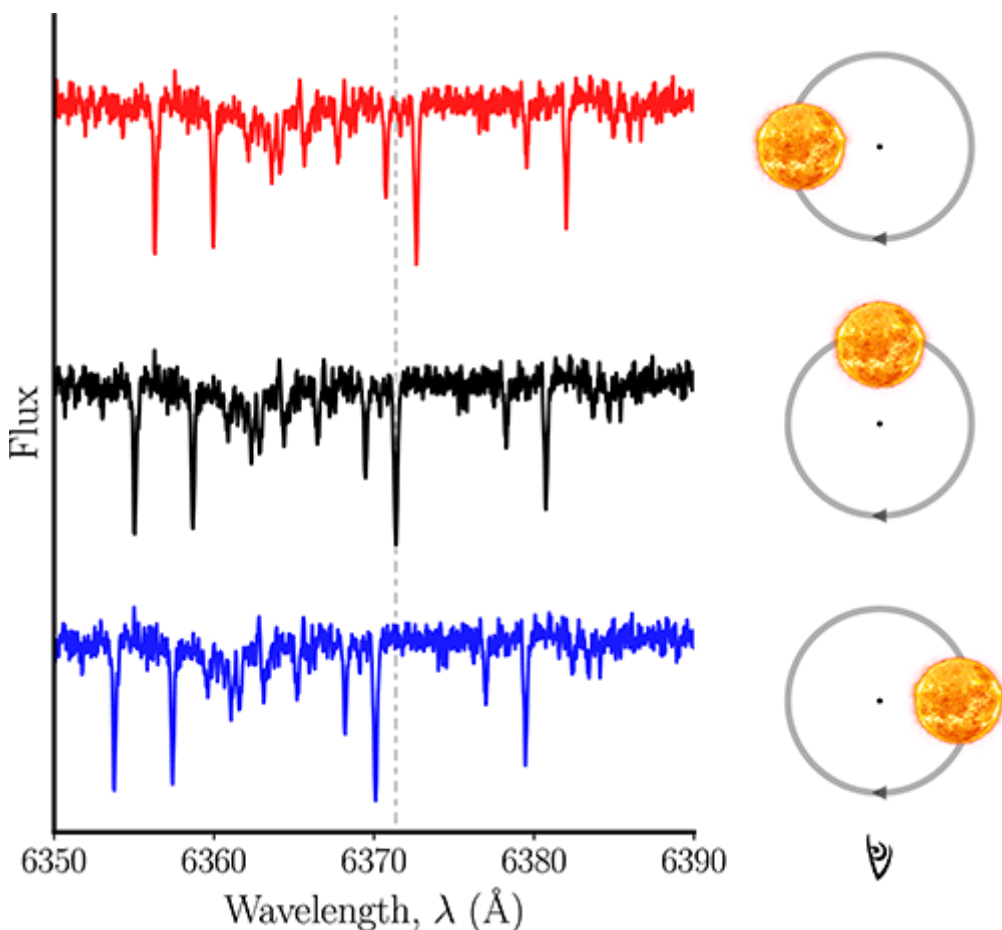


Figure 1. Illustration of the Doppler effect on a portion of a stellar spectrum. As the star orbits the center of mass, the spectrum is red-shifted and blue-shifted relative to the position of reference spectral lines.

In this representation, the observer is at the bottom of the plot, as indicated.

To circumvent the difficulties involved in the detection of such low amplitude signals, two main aspects must be taken into account. First, the typical spectrum of a solar-type star has thousands of well-defined absorption lines. Using this information statistically, one will be able to achieve the necessary precision. But this is not enough if the spectrograph itself is not stable, or if one cannot control the instrument drifts as a function of time. An accurate way to measure and control the wavelength-to-pixel calibration is thus needed. This is usually achieved using the spectrum of a calibration source that is obtained simultaneously with the target spectrum (e.g., Baranne et al., 1996), or using a gas cell whose spectrum is superposed with the spectrum of our star (e.g., Campbell, Walker, & Yang, 1988). For reference, the most precise existing RV instrument is the ESPRESSO spectrograph (Pepe et al., 2014) at the ESO-VLT telescope (for a review of several spectrographs used in radial velocity measurements see (Fischer et al., 2016)). ESPRESSO is expected to measure long-term RVs with a precision better than 10 cm/s.

Highlights from the Radial Velocity Method

While using Doppler spectroscopy to detect exoplanets is an old concept (e.g., Belorizky, 1938), the measurement precision on stellar radial velocities only reached the *planetary* level in the late 1980s. At that time, the first tentative detections of low mass companions orbiting solar-type stars were announced, even if cautiously (e.g., Campbell et al., 1988; Hatzes & Cochran, 1993; Latham, Mazeh, Stefanik, Mayor, & Burki, 1989). But the first unambiguous detection of an exoplanet orbiting another “sun” would have to wait until 1995, when the discovery of 51 Pegasi b was announced (Mayor & Queloz, 1995). This planet is a hot Jupiter, with a minimum mass of $0.47 M_{Jup}$ and orbiting at 0.05 AU from its host star every 4.2 days. Several detections of similar planets quickly followed (e.g., Butler & Marcy, 1996; Marcy & Butler, 1996). Around one of the first planet-host stars, Upsilon Andromedae, one would eventually find not just one but three orbiting planets (Butler et al., 1999): the first example of a multi-exoplanet system. These early detections targeted solar-type stars (FGK dwarfs), but some RV surveys also started targeting M stars, resulting for example in the detection of a giant planet around the close-by M4 dwarf Gl 876 (Delfosse et al., 1998; Marcy, Butler, Vogt, Fischer, & Lissauer, 1998).

Further improvements in RV precision and the use of dedicated observing strategies allowed for the detection of the first planets in the Neptune or Super-Earth mass range: mu Arae c (Santos et al. 2004, GJ 436 b Butler et al. 2004, and 55 Cnc e McArthur et al. 2004). Over the last decade, with the accumulation of precise RV observations, the lower limits in planet mass have steadily decreased (e.g., Delisle et al., 2018; Pepe et al., 2011).

Some particular detections gathered the attention of the media and the general public. The Sun’s closest stellar neighbor, Proxima Centauri, was announced to host a planet with a minimum mass of only $1.3 M_{\oplus}$ (Anglada-Escudé et al., 2016). At an orbital distance of around 0.05 AU, the planet is within Proxima’s habitable zone, where water could be in the liquid state (Ribas et al., 2016; Tabet et al., 2016).⁴ Planets were also detected around two other of our close neighbors, Ross 128 (Bonfils et al., 2018) and Barnard’s star (Ribas et al., 2018). The first is a $1.35 M_{\oplus}$ super-Earth orbiting close to the habitable zone, while Barnard b has $3.23 M_{\oplus}$ and a long orbital period of 232 days. This particular detection relied on several hundred RV observations from different instruments, and highlights the difficulty in finding such low amplitude signals.

At the time this review is written, the lowest masses so far measured by RVs belong to the companions of YZ Cet, a low-mass M4 dwarf located 12 light-years from the Sun (Astudillo-Defru et al., 2017). This system hosts at least three planets with mass compatible with Earth’s but in a very compact configuration (orbital periods of 1.97, 3.06, and 4.66 days). Perhaps more importantly, all these detections of planets orbiting the closest nearby stars to our Sun show that planets are ubiquitous in our Galaxy.

Following up on the incredibly successful transit surveys, such as CoRoT, WASP, and Kepler, the RV technique has shifted part of its focus from discovery to confirmation and characterization. Many of the lowest mass planets detected so far, were first found in photometry and later confirmed with RVs (e.g., Jontof-Hutter, Rowe, Lissauer, Fabrycky, & Ford, 2015; Pepe et al., 2013; Queloz et al., 2009; Weiss et al., 2016).

Transit Photometry

High precision photometry allows detection and characterization of planets orbiting other stars using an approach that is conceptually simple. When a planet crosses the stellar disk (as seen by the observer), it will block part of the stellar light. This *transit* (in analogy with the transit of the inner solar system planets Mercury and Venus in front of the Sun) can be observed if the orbital axis of the planet is close to perpendicular to our line of sight. For a given system, the geometric transit probability (p) can be expressed in good approximation by:

$$p = \frac{R_{star}}{a} \quad (7)$$

In this equation, R_{star} and a are the stellar radius and the planetary orbital radius, respectively. This formula is valid for a circular orbit (for a more detailed description and equations refer to Winn, 2018).

From the equation, it can be seen that, as for the radial velocity method, the transit technique is also more sensitive to short period planets. While for a 3-day orbital period planet p is close to 10%, for a planet at 1 AU from its parent star (orbital period close to 1 year), p goes down to only 0.5%. Although these numbers seem small, continuous surveys of large numbers of stars in the sky provide a significant number of detections.

If a transit event is observed, the expected relative luminosity variation $\Delta L/L$ (the relative amount of light that is blocked by the disk of the planet) relates with the planet and stellar radii

(R_{planet} and R_{star} , respectively) through the following equation:

$$\frac{\Delta L}{L} = \left(\frac{R_{planet}}{R_{star}} \right)^2. \quad (8)$$

For a Jupiter-like planet orbiting a solar-like star, $R_{planet} \sim 0.1 R_{star}$, thus inducing a photometric variation of the order of 1%. A value of the order of 100 parts per million (ppm) is expected for an Earth radius object transiting a solar-type star. Large planets orbiting smaller stars are thus easier to detect using the transit method. An illustration showing the transit geometry and the parameters that can be derived from a transit is shown in Figure 2.

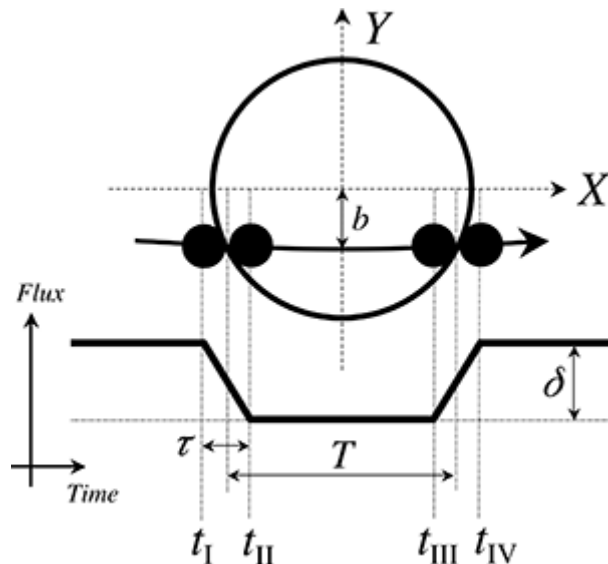


Figure 2. Illustration showing the parameters that can be derived from a transit: the impact parameter b , the transit depth δ , the transit duration T and the ingress/egress time τ .

Figure adapted from Seager and Mallén-Ornelas (2003).

As illustrated in the figure, the transit shape can be defined by four contact points. The first contact point is when the planet radius just overlaps with the stellar radius (t_I), and the second contact point is when the full disc of the planet covers the star (t_{II}). The event from t_I to t_{II} is called ingress. The third contact point is when the planet radius starts to uncover the stellar disc (t_{III}). The forth contact point is when the planet disc stops covering the stellar disc (t_{IV}). The event from t_{III} to t_{IV} is called egress. The transit duration is the time it takes from t_I to t_{IV} , while the duration of the full transit is the time from t_{II} to t_{III} .

From Figure 2 it can also be inferred that the transit duration and ingress/egress times depend on three parameters: the planet-to-star radius ratio ($R_{\text{planet}}/R_{\text{star}}$), the ratio between the planet-to-star distance and the stellar radius (a/R_{star}), and the impact parameter (b).⁵ It can be shown (Seager & Mallén-Ornelas, 2003) that for circular orbits, combining the transit duration, the ingress/egress time, and the transit depth allows to derive the planet-to-star radius ratio, the planetary orbital inclination, and stellar density. For eccentric orbits, this is also possible if the eccentricity and argument of periastron (ω) are known.

Further to the parameters mentioned above, the exact shape of the transit light curve also depends on the properties of the stellar disk and its flux distribution, including the limb darkening of the star. As such, although there are analytic formulas to describe the transit shape, due to the complex geometry of the system, the exact shape of the transit light curve is not straightforward to model with a simple analytical function (for details and references see, e.g., Winn & Fabrycky, 2015), even if significant progress has been done toward that (Agol, Luger, & Foreman-Mackey, 2020). As such, the modeling is usually done with available algorithms and software libraries (e.g., Mandel & Agol, 2002). The existence of a planetary atmosphere may also change this curve.

The transit method was shown to be an excellent way to detect planets orbiting other stars. At first used to complement the detections of radial-velocity planets (e.g., Charbonneau, Brown, Latham, & Mayor, 2000), large ground and space-based surveys, like OGLE, WASP, HAT-P, CoRoT, Kepler, and TESS revealed the presence of thousands of candidates, several with radii smaller than the Earth. However, one point that is clear is the fact that the transit method only provides information about the radius of the planet. In fact, the transit light curve has no information about the planet mass, except in a few cases where the timing of the transit changes as a result of significant interactions between planets in multi-planetary systems (e.g., Ford et al., 2012). In other words, given the diversity of possible chemical compositions, and the strong degeneracy existing in the mass-radius relation, to characterize the planet in more detail one usually needs to use a method (e.g., radial velocities) to derive the planet mass.⁶

Interestingly, in planetary systems with more than one planet, the planets' mutual gravitational interactions perturb each other's orbit, giving rise to transit timing variations (TTVs). For planets near mean-motion resonances (MMR), the perturbations are large enough to be detected. However, a long baseline of observations is usually needed, since the period of the perturbations is much longer than the orbital period of the outer planet. This libration period or super period is related to the resonant angles, which measure the displacement of the longitude of the conjunction from the periapsis of each planet. As mentioned, TTVs thus provide another method to estimate planetary masses, which is related to the TTV amplitude. In general, the TTV curve is periodic and the inversion of the TTVs to derive the planetary masses relies on a good sampling of one libration cycle. Therefore, the long baseline of Kepler (Borucki et al., 2011) was needed to detect and characterize TTVs in systems.

Finally, it is well known that different *non-planetary* phenomena can produce signals that almost perfectly mimic a photometric transit. These are responsible for large false positive rates in most transit surveys (e.g., Burke, Mullally, Thompson, Coughlin, & Rowe, 2019; Morton & Johnson, 2011; Santerne et al., 2016; Torres et al., 2011). Complementary observations are thus usually needed once a transit signature is detected, even if a statistical confirmation is also used in many cases (Díaz et al., 2014; Morton, 2015; Torres et al., 2015), especially when dealing with transits on very faint stars, like most Kepler candidates, for which follow up observations (e.g., radial velocities) are not possible.

Highlights from the Transit Method

The first exoplanet discovered to transit its host star, HD209458 b (a planet previously detected through radial velocities), is a hot Jupiter (Charbonneau et al., 2000). This discovery raised the degeneracy between mass and orbital inclination and confirmed that the unexpected "hot-jupiters" were real planetary mass objects. These giant planets, similar to Jupiter but in very short period orbits, were initially difficult to explain based on traditional planet formation processes, leading to an initial scepticism about their true nature.

The efficiency of transit surveys has been demonstrated by the Kepler mission (Borucki et al., 2011) that discovered several thousands of planets, a significant part of which are confirmed or statistically validated. Kepler has revealed exoplanets around a diversity of hosts from M-dwarfs (Dressing & Charbonneau, 2015) to giant (Quinn et al., 2015) and binary stars (Doyle et al., 2011). Several planets were found in the habitable zone (Batalha et al., 2013).

Furthermore, Kepler's results found that the most common planets with periods shorter than \sim 85 days are super-Earths and mini-Neptunes (Fressin et al., 2013), confirming previous suspicions from radial velocity surveys (e.g., Mayor et al., 2014). The smallest planet found by Kepler is Kepler-138b (Jontof-Hutter et al., 2015), with a size similar to Mars. It has a radius of $0.522 R_{\oplus}$, a mass of $0.066 M_{\oplus}$, and it orbits its host star every 10.3 days. The host star has half of the mass of the sun and less than half of its radius, which makes the planet detection and characterization easier. Moreover, there are two other planets in the system, with the three planets making a resonant chain that allowed the derivation of the planetary masses from the modeling of the transit timing variations. Due to the faintness of the host star ($V=13$ mag), it is challenging to derive the planetary masses through radial velocity measurements.

In 2014, after two reaction wheel failures, the Kepler spacecraft had to adapt its observing strategy and was transformed into the K2 mission, observing brighter targets close to the ecliptic. The smaller observing duration of each K2 field (\sim 80 days) compared with the 4 years duration of the Kepler mission, was compensated by the larger number of stars and hence the larger number of brighter targets, leading to new and interesting discoveries. One of the planets discovered by this mission was K2-288B b (Feinstein et al., 2019), which orbits the smaller component of a low mass binary star. The host star is approximately one third the size of the Sun. The planet has a radius of $1.9 R_{\oplus}$, and it orbits the host star every 31.39 days. Because the host star is low mass, and hence it has much lower temperature and luminosity than the Sun, the planet is thought to be cooler than the Earth with an equilibrium temperature of $-41^{\circ} C$. Another interesting fact about this planet is that it was discovered by citizen scientists with the exoplanet explores project. This project was built on the successful planet hunter project (Fischer et al., 2012). In these projects, citizen scientists look at thousands of light curves by eye to identify the signals produced by planets.

Another interesting system is Trappist-1, discovered by the ground-based Trappist survey (Gillon et al., 2011). Using the Trappist high precision photometric observations, three short period Earth-size transiting planets were found orbiting the ultra cool dwarf (M8-type) Trappist-1 (Gillon et al., 2016). Later, a long observing run (20 days) with the Spitzer space telescope and several ground based follow-up transit observations revealed the existence of 4 more planets (Gillon et al., 2017), making this exoplanetary system one with the highest number of known planets—Kepler-90 is the record holder with 8 planets (Shallue & Vanderburg, 2018). An example of a triple transit of planets c, e, and f is given in Figure 3. The longest period planet was only constrained using further K2 observations (Luger et al., 2017). The planets have periods of 1.51, 2.42, 4.04, 6.06, 9.1, 12.35, and 18.77 days and radii between $0.755 R_{\oplus}$ and $1.127 R_{\oplus}$. Hence, this is an extremely compact system with a star that is only slightly larger than Jupiter and has only 0.08 solar masses. However, due to the strong tidal effects on such compact systems that circularizes and synchronizes the orbit of the planet, it is possible that any liquid water that existed would have evaporated.

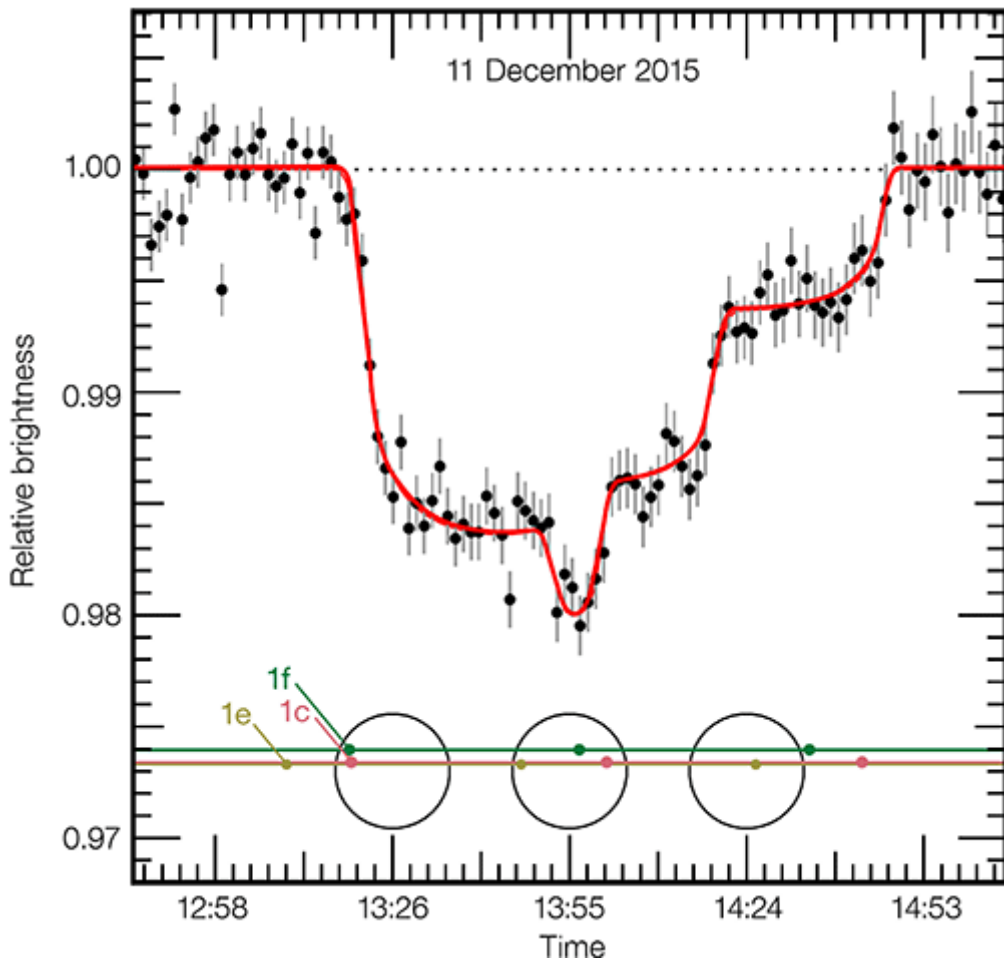


Figure 3. Triple transit of Trappist-1 planets c, e and f observed by HAWK-I at the very Large Telescope.

Figure adapted from Gillon et al. (2017).

Combining Transits and RVs

For transiting exoplanets, it is possible to derive the radius of the planet (through transit observations) and the mass of the planet (mainly through radial velocity observations). Hence, the bulk density of the planet can be estimated with good accuracy, giving insight into its composition and internal structure (e.g., Fortney, Marley, & Barnes, 2007; Guillot, Santos, Pont, Iro, Melo, & Ribas, 2006).

Formation and compositions theories predict that planets are made of four main components: H/He, water/ices, silicates, and iron/nickel (e.g., Seager et al., 2007). Different combinations of these materials result in a wide range of possible radii for a given planetary mass. Planets larger than Neptune are expected to be mainly gaseous. Planets similar or smaller than the Earth are expected to be rocky, while planets with sizes between 1.5 and $4 R_{\oplus}$ can have compositions ranging from gaseous mini-Neptunes, to water worlds, down to rocky Super Earths (Léger et al., 2004; Rogers, 2015; Rogers, Bodenheimer, Lissauer, & Seager, 2011; Seager et al., 2007; Valencia et al., 2006).

Due to the faintness of the host stars in the *Kepler* field, it was only possible to derive accurate masses for relatively few of the *Kepler* candidates in the small radii regime. Nevertheless, *Kepler* revealed a large diversity of planetary compositions (Barros et al., 2014, 2017; Carter

et al., 2012; Dressing & Charbonneau, 2015; Haywood et al., 2014; Marcy et al., 2014; Santerne et al., 2018). Figure 4 shows the mass-radius diagram for known exoplanets. Interestingly, it is clear that planets with very similar radii can have very diverse densities—for example, Kepler-11f ($\rho = 0.7 \pm 0.4 \text{ g cm}^{-3}$, $r_p = 2.61 \pm 0.025$; Lissauer et al., 2011) and Kepler-10c ($\rho = 7.1 \pm 1.0 \text{ g cm}^{-3}$, $r_p = 2.35 \pm 0.05$; Dumusque et al., 2014).

Figure 5 shows an example of the data used for the detection and characterization of a planetary system discovered by Kepler-K2 and confirmed with radial velocities K2-229 (Santerne et al., 2018). The K2 light curve shows transits of three planets with periods 0.58 days, 8.32 days, and 31.0 days. Radial velocities obtained with the HARPS spectrograph allowed researchers to derive the mass of planet b and c and hence estimate their density. The inner planet has a mercury-like composition. K2-229 is an active star and stellar variability is present both in the light curve and in the radial velocities. Gaussian process regression was needed to correct the stellar variability and derive robust radii and masses.

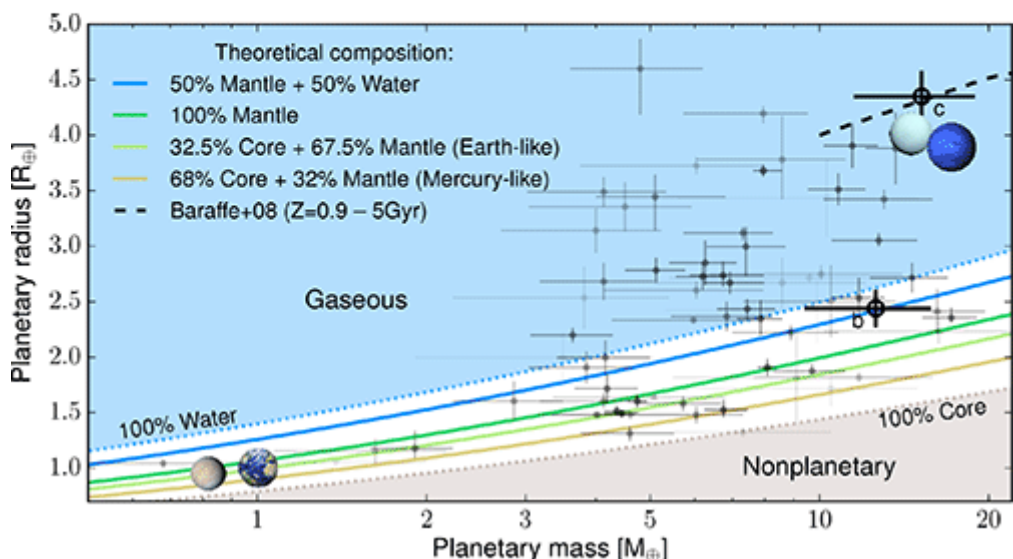
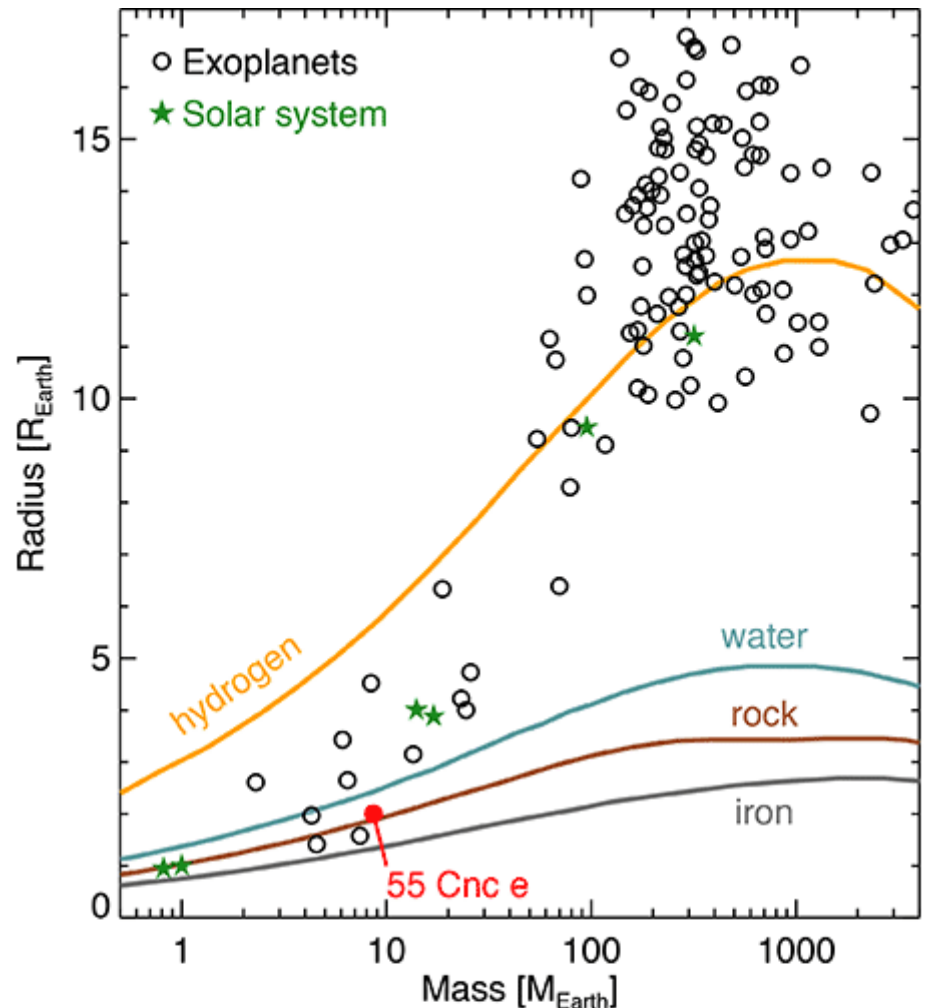


Figure 4. Top: Overview of the masses and radius of known transiting exoplanets and solar system planets around the time of the discovery of 55 Cnc e. Adapted from Seager, Kuchner, Hier-Majumder, & Militzer, 2007; Winn, 2011. Bottom: Zoom for the low mass regime of the masses and radius of known transiting exoplanets. We overplot different compositions for solid planets in between pure iron and pure water. The black dashed line corresponds to the models of Baraffe, Chabrier, and Barman (2008) for gaseous planets with heavy material enrichments of 0.9 and an age of 5 Gyr. We superimposed the known planets in this mass-radius range where the greyscale depends on the precision of the mass and radius.

Adapted from Barros et al. (2017).

Using a sample of Kepler planets for which it was possible to derive precise masses, Rogers (2015) has shown that most planets larger than $1.6 R_{\oplus}$ are not rocky. Furthermore, another study revealed the existence of a gap in the radius distribution of Super-Earths (Fulton et al., 2017).⁷ This gap is located at $1.8 R_{\oplus}$ (close to the value mentioned above) and divides a population with a peak at $\sim 1.3\text{--}1.5 R_{\oplus}$, which includes planets with densities similar to rocky worlds and a population with a peak at $\sim 2.3\text{--}2.5 R_{\oplus}$, with clearly lower densities. This gap has been proposed to be due to photo-evaporation of the atmospheres of low mass planets at high stellar irradiation (e.g., Owen & Wu, 2017; Van Eylen et al., 2018). Indeed, it was shown recently that the gap position is closer to the star for lower mass stars. This is in agreement with the photo-evaporation hypothesis, as low mass stars have higher X-ray emission than their more massive counterparts (Fulton, Petigura, Blunt, & Sinukoff, 2018). The existence of a radius gap supports the transition between rocky planets gaseous planets found by Rogers (2015). This transition and its width depends on the place of planet formation and its subsequent migration, given that planets formed beyond the water ice line are expected to have higher water mass fraction, between 30 and 40%, and higher H/H₂ fraction (10–20%) (Thiabaud, Marboeuf, Alibert, Leya, & Mezger, 2015). Probing the transition zone between rocky and gaseous planets as a function of stellar distance will help constrain planetary formation and migration models.

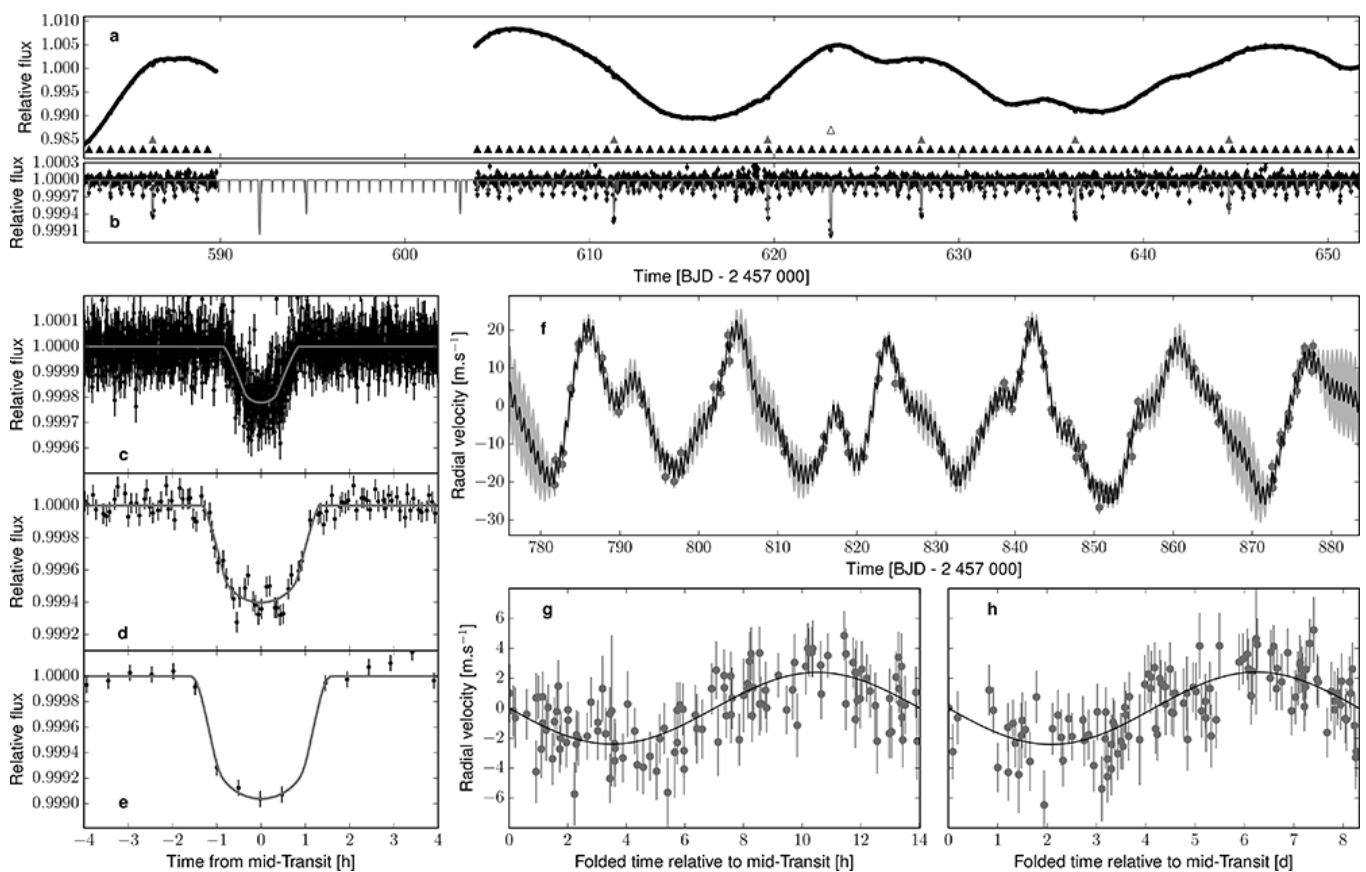


Figure 5. Photometric and RV data of the K2-229 system. The different panels show the K2 light curve (a), with the transits of planets b, c, and d indicated by the triangles. Panels (c), (d), and (e) show phase-folded transit light curves of the planets b, c, and d (respectively). In panel (f) the RV time series obtained with HARPS is shown together with the best 3-Keplerian orbit and a Gaussian process regression. Panels (g) and (h) show the phase-folded RV data. From Santerne et al. (2018).

The relation between transiting planets and radial velocities goes beyond the measurement of planet masses. For transiting exoplanets, is it also possible to measure the sky-projected angle between the stellar rotation and the planetary orbit axis, through the Rossiter-McLaughlin effect (e.g., Winn, 2011). Such a measurement provides fundamental information about the formation of planets. For the Solar System case, for example, all planets have orbital planes close to the solar equator, a result that is expected from standard planet formation models.

The first planets for which the Rossiter-McLaughlin effect was measured were found to have orbits well aligned with the stellar rotation axis. However, after the discovery of the first misaligned system (Hébrard et al., 2008), many others followed. Measured obliquities (the sky projected angle between the stellar rotational axis and the orbital angular momentum vector) in hot-Jupiters brought a new insight into hot-Jupiter migration mechanisms, as well as about the interaction between the star and the planet. Such processes can alter and shape the geometry of the planetary systems. It was shown that hot-Jupiter host stars obliquities depend on the tidal dissipation timescale (Albrecht et al., 2012). Low obliquity systems have short tidal dissipation timescales, while high obliquity systems have high tidal dissipation timescale. This suggests that obliquities are initially random which is expected if hot Jupiters migrate through high eccentricity tidal migration (Ford & Rasio, 2008; Rasio & Ford, 1996; Weidenschilling & Marzari, 1996;). However, some hot-Jupiters could also be formed by disc migration (Dawson & Johnson, 2018).

From the equations in previous sections, it is clear that planet properties, as derived from the radial velocity and transit methods, depend on our knowledge of the star. The mass derived from the RV measurements is dependent on our knowledge of the stellar mass, while the transit light curve only allows to derive the planet-to-star radius ratio: independent knowledge about the stellar radius is thus fundamental. In this context, GAIA DR2 (Gaia Collaboration et al., 2018) provided parallaxes for most of the exoplanet host stars. The stellar parallaxes allow a significant decrease of the uncertainty in stellar radius. For example, for the sample used to probe the Super-Earths gap discussed above it allowed the decrease of the uncertainties on the stellar radius from 11 to 2%.

These simple examples illustrate how relevant the study of stellar astrophysics is in the exoplanet domain. We point the reader to Santos and Buchhave (2018) for a review on the full relevance of understanding characterizing and understanding of planet-host stars. As discussed in the next section, This importance actually goes far beyond planet characterization.

Detecting Planets: The Challenges of Signal Analysis

Despite the success of our search for exoplanets, there are still a number of challenges hindering the detection of planets in both RVs and photometry. Intrinsic stellar noise is a long-recognised problem in planet search programs. The signals produced by magnetic activity features such as spots and plages (in both RV and photometry) can prevent the finding or correct characterization of the planets' orbital parameters, or can even produce false detections (e.g., Figueira et al., 2010; Queloz et al., 2000; Rajpaul, Aigrain, & Roberts, 2016). Because of the different timescales and observables, the RV and transit techniques deal with stellar noise in slightly different ways.

Radial Velocities

The presence of active regions on the stellar surface is known to cause large-amplitude RV variations (Saar & Donahue, 1997; Santos et al., 2000). Furthermore, the acoustic modes of solar-type stars, the atmospheric granulation motions, and long-term magnetic cycles (like the solar 11-year cycle), can also induce RV variations on the order of a few m/s (e.g., Cegla, Watson, Shelyag, Mathioudakis, & Moutari, 2019; Díaz et al., 2016; Dumusque et al., 2012; Kjeldsen et al., 2005; Meunier & Lagrange, 2019).

To try to circumvent this problem, active stars are often discarded from RV surveys. However, the discovery of small transiting planets around active stars means that one has to deal with the stellar activity contaminations. A number of methods were developed to do so, either based on a custom observational strategy (e.g., Dumusque, Santos, Udry, Lovis, & Bonfils, 2011a; Dumusque, Udry, Lovis, Santos, & Monteiro, 2011b), auxiliary spectral indicators of activity (e.g., Bonfils et al., 2007; Desort, Lagrange, Galland, Udry, & Mayor, 2007; Figueira, Santos, Pepe, Lovis, & Nardetto, 2013; Lanza et al., 2018; Queloz et al., 2001), simultaneous photometric observations (e.g., Boisse et al., 2009; Giguere et al., 2016; Haywood et al., 2014; Oshagh et al., 2017), or careful modeling of the RV time series (e.g., Cloutier et al., 2019; Hatzes, 2014; Hatzes et al., 2010; Rajpaul, Buchhave, & Aigrain, 2017).

Sophisticated statistical methods have also been developed to model the activity-induced signals as correlated (or *red*) noise. Earlier work on this front (Baluev, 2013) started a long history of contentious studies on the planetary nature of signals found in RV time series (e.g., Anglada-Escudé et al., 2013; Faria et al., 2019; Jenkins & Tuomi, 2014; Robertson & Mahadevan, 2014; Santos et al., 2014). More recently, Gaussian processes (GPs) became an important tool in the planet-hunting arsenal (Cloutier et al., 2017; Faria et al., 2016; Grunblatt, Howard, & Haywood, 2015; Haywood et al., 2014). These non-parametric models of correlated noise can account for some of the expected characteristics of stellar activity signals, such as their quasi-periodicity. By including physically-meaningful parameters in the GP covariance function, which can be related to the stellar rotation period and the timescale of evolution of the active regions, these models can also be used to infer such stellar characteristics (e.g., Cloutier et al., 2017; Damasso & Sordo, 2017; Haywood et al., 2014).

Even without the confounding variations from stellar activity, the analysis of RV time series is still problematic due to the interplay of complicated time sampling (which creates spurious aliases; see e.g., Rajpaul, Aigrain, & Roberts, 2016), the nonlinear nature of the Keplerian curve (e.g., Wittenmyer, Bergmann, Horner, Clark, & Kane, 2019a), and the difficulty in statistically comparing models with different number of planets (e.g., Feroz, Balan, & Hobson, 2011; Tuomi & Jones, 2012). The community has recognized the appeal of Bayesian methods to help solve some of these issues (Dumusque et al., 2017; Fischer et al., 2016;), even though the development of new statistical methods is still a very active area of research (Baluev & Shaidulin, 2015; Faria, Santos, Figueira, & Brewer, 2018; Hara, Boué, Laskar, & Correia, 2017).

Transits

In order to detect transiting planets, three important steps are required: light curve filtering, transit search, and vetting. Light curve filtering includes the correction of instrumental noise and the removal of stellar variability. There are several filters that have been applied over the years. Their success relies on the fact that the transit time scale is usually very different from the instrumental noise and stellar variability timescales. Further to this, note that the transit signal only affects a short portion of the light curve, contrasting with the radial velocity signal, which is much harder to decouple from stellar variability, as mentioned. Usually, the filtering includes sigma clipping of the outliers, a high pass filter to correct the low frequency noise coming from stellar activity, and a low pass filter to remove high frequency variations. Examples of high pass filters are sliding mean and spline filter (e.g., Barros, Demangeon, & Deleuil, 2016) used to remove variability with timescales longer than ~ 1 day.⁸ One commonly used low pass filter is the Savitzky-Golay filter (Press, Teukolsky, Vetterling, & Flannery, 1992) with a time scale of $\sim 1\text{ h}$ to preserve transit ingress and egress. On top of frequency filters, more sophisticated methods have also been used to filter the light curve, like for example, the wavelets-based adaptive-matched filter Jenkins (2002) and Gaussian processes (Aigrain, Hodgkin, Irwin, Lewis, & Roberts, 2015).

After filtering the light curve, the transit search is performed with some variation of a box-fitting least-squares (BLS) algorithm (Kovács, Zucker, & Mazeh, 2002). The search is made over periods ranging from the shortest expected planet period, up to a period equal to the duration of the observations. For each trial period, the light curve is phase folded and binned. Then the algorithm searches for box shape signal at different trial epochs (phase). The depth and duration of the box signal is fitted, and the best fit of each trial period is selected. The signal-to-noise of the best fit as a function of the trial period produces a periodogramme that peaks at the most likely planetary orbital periods. For each light curve the signal detection efficiency (SD) is computed (see e.g., Kovács et al., 2002) and compared with a threshold above which a signal is considered as a significant transit detection. The planetary candidates that pass the threshold are then vetted.

Several instrumental and astrophysical phenomena can produce transit like events and hence the detections need to be vetted using several criteria which comprises the third step. To eliminate instrumental noise, the light curves are often inspected by eye. To eliminate astrophysical false positives, several indicators are automatically computed and used in automatic and semi-automatic vetting. Astrophysical false positives are usually due to the existence of another star in the photometric aperture, though a plethora of other situations can occur (e.g., Santerne et al., 2013). This can be due to a chance alignment or the existence of a gravitationally bound system (binary, triple systems). Usual signs of astrophysical false positives are: variations of the photo-center (“centroid”), sinusoidal out-of-transit variations, significant difference between odd and even transits, existence of a significant secondary, or transit depth variations with photometric filter. Complementary information, such as spectral type of the host star, is also useful when checking false positives. For instance, the stellar density can be inferred from the transit light curve itself (e.g., Winn & Fabrycky, 2015) and compared with the density of host star inferred from spectral analysis and modeling. Some types of false positives can only be found using radial velocity follow-up observations. Hence,

transit candidates usually required RV observations to be confirmed, although when this is not possible, statistical validation can be applied in some cases (Díaz et al., 2014; Morton, 2012; Torres et al., 2011).

Recently, automatic methods for transit planet search and transit planet vetting have been developed based on machine learning algorithms. For detecting transits, deep learning was proposed (Zucker & Giryes, 2018), and for vetting candidates, several algorithms were applied to ground-based surveys such as WASP (Schanche et al., 2019), Kepler (Armstrong, Pollacco, & Santerne, 2017; McCauliff et al., 2015; Shallue and Vanderburg, 2018; Thompson et al., 2018), and TESS (Osborn et al., 2019).

One should add, however, that even after all this analysis, stellar activity can still affect the modeling of the transit light curve (e.g., Barros et al., 2013, 2014; Oshagh et al., 2013a,b). Other stellar sources of noise also exist (e.g., granulation Barclay et al., 2015), that can affect the precision of the measurements and the subsequent derivation of planetary physical parameters.

Other Methods for Planet Detection and Characterization

The next sections discuss other methods that have a strong potential to play a relevant role in exoplanet detection, in particular for the detection and characterization of rocky planets orbiting nearby solar-type stars. For a more detailed description of other planet detection and characterization methods the reader can follow some other reviews (Perryman, 2018; Seager, Dotson, Lunar, & Planetary Institute, 2010).

Astrometry

The motion of the star around the center of mass of the star planet system (the basic principle discussed above for the radial velocity method) also produces a motion on the plane of the sky. This induces a small periodic astrometric shift of the stellar position, seen as a wobble against fixed background distant objects. This astrometric detection of an extra-solar planet can be described, in a very basic approach, by simple physics. The semi-major axis of the orbital motion of a star about the center of mass of a two-body system is given by:

$$M_1 a_1 = M_2 a_2 \quad (9)$$

where M_1 and M_2 are the masses of the two bodies, and a_1 and a_2 the semi-major axes of their orbits. The distance $a = a_1 + a_2$ (the semi-major axis of the relative orbit) is also related to the orbital period P by Kepler's third law,

$$P^2 = \frac{a^3}{M_1 + M_2} \quad (10)$$

where P is in years, a in astronomical units, and the masses M_1 and M_2 in solar masses. In principle, if one measures a_1 , a_2 , and P , the system above can be solved to derive the mass of the two bodies. This is the case for some visual binary stars. The detection and characterization of a planet using astrometry is, however, far more complex than denoted by these equations. For instance, given that the planet is usually not seen, one can only hope to measure a_1 and the period P .⁹ To solve the above system and derive the mass for the planet, one needs for example to estimate the mass of the star (M_1) using stellar evolution models.

As can be seen from equation (10), the semi-major axis of the astrometric motion of the star around the center of mass of the star-planet system is proportional both to the mass of the companion and to its orbital period. This means that the astrometric technique is most sensitive to long period (massive) companions. Astrometry is in this sense complementary to the radial-velocity or transit techniques.

In a more general way, the motions in right ascension and declination of the star can be denoted by the following equations:

$$\zeta = \alpha_0 + \mu_\alpha (t - t_0) + P_\alpha \pi + y \quad (11)$$

$$\eta = \delta_0 + \mu_\delta (t - t_0) + P_\delta \pi + x \quad (12)$$

where α_0 and δ_0 are the position in right ascension and declination at a reference time t_0 , respectively, μ_α and μ_δ are the proper motions (in the two coordinates), P_α and P_δ the terms related with Earth's parallax. Finally, x and y are the terms that include the perturbation produced by the orbiting planet. These are shown to be expressed by:

$$x = AX + BY \quad (13)$$

$$y = BX + GY \quad (14)$$

where $X = \cos E - e$ and $Y = \sqrt{1 - e^2} \sin E$, and A, F, B, and G are the Thiele-Innes parameters. These are functions of the semi-major axis of the orbit, the orbital inclination, the argument of periastron, and the longitude of the ascending node. Refer to Hilditch (2001) for more details.

Overall, as seen from equations 11 and 12, the effect produced by the planet's tug is just one of several relevant that have to be derived simultaneously to model the astrometric motion of the star (namely together with the *apriori* unknown values of the proper motions). It is also instructive to quantify the values of the different terms in equations 11 and 12. For a typical

nearby star, typical values of the proper motions are 30 mas yr⁻¹, while Earth's parallax produces a 1-year period wobble with an amplitude of the order of 60 mas. At 10 pc from the Sun, a giant planet in a Jupiter-like orbit will induce an amplitude of x and y of the order of 0.5 mas. This illustrates the challenge of using astrometry to detect planets orbiting other stars.

Given the small expected astrometric motions, the astrometric method has not been very successful in the discovery of exoplanets. The only existing detections are of planets or brown-dwarfs first detected using the radial-velocity technique (e.g., Benedict et al., 2006). More hopes come from the analysis of data from the GAIA (ESA) mission, whose exquisite astrometric precision is expected to allow the detection of thousands of giant planets in long period orbits (Sozzetti, Casertano, Lattanzi, & Spagna, 2001).

Direct Imaging

The adjective *direct* for the detection or characterization of exoplanets refers to every method that aims to detect the photons emitted or reflected by an exoplanet. These methods are opposed to *indirect* methods that rely on stellar photons to detect the secondary effects of the presence of an exoplanet. During the early days of exoplanetology, the distinction was clear between indirect and direct methods. Radial velocities, transit photometry, astrometry, and microlensing¹⁰ constituted the indirect methods, while direct imaging and nulling interferometry constituted the direct methods. Nowadays, the separation is blurrier. Transit photometry has been used to measure secondary eclipses and orbital phase curves (e.g., Knutson et al., 2007). Correlation techniques applied to high resolution spectra have been used to detect absorption lines in the emitted (e.g., Snellen, de Kok, de Mooij, & Albrecht, 2010b) and reflected (e.g., Martins et al., 2015) spectra of exoplanets. However, direct imaging (DI) is the only direct observing technique that is used to discover (as opposed to characterize) exoplanets. As the name suggests, DI relies on the most intuitive way to detect an exoplanet: produce a resolved image, separating the image of the star from that of the planet. For that purpose, two obstacles have to be overcome: contrast and angular separation. For this reason, DI is often referred to as a high contrast and high angular resolution technique.

To produce a resolved image of an exoplanet, one needs to separate the planet from its closest light source, its parent star. The minimum required angular separation is given by the ratio of the star-planet distance over the distance that separates the system from us. DI is thus more suited to explore the outer system of stars in the neighborhood of the Sun. To give orders of magnitude, from the ground, angular resolution is limited by the turbulent atmosphere to typically ~ 1 arcsecond. The minimum angular resolution required to resolve a planet orbiting at 1au from its parent star located 10pc away from the observer is ~ 100 mas. As a consequence, DI from the ground relies on adaptive optics (AO) to correct for the distortion of the wavefront produced by the atmosphere and recover the diffraction limited angular resolution.

The diffraction limited angular resolution is given by the Rayleigh criteria (e.g., Hecht, 2002) and is proportional to the ratio of the wavelength of observation over the size of the entrance pupil of the telescope (λ/D). It corresponds to the angular size of the Airy disk, which is the central lobe of the point spread function (PSF) of an ideal circular aperture telescope. The full

(PSF) of such a telescope is described by the Airy disc function (Airy, 1838). For a 10m class telescope like the VLT, the diffraction limited angular resolution is \sim 50 mas in the near infrared. The two main components in an ao system are the wavefront sensor, which measures the distortions induced by the atmosphere, and the deformable mirror, which compensate them. Its performances are measured by the Strehl ratio (Strehl, 1902). It is defined as the ratio between the amplitudes of the peaks of the AO corrected point spread function (PSF) and the ideal PSF (which would be observed without atmosphere). Current AO can reach Strehl ratios of $\sim 90\%$.

Angular resolution alone is not enough. The Rayleigh criteria used to quantify the angular resolution of a telescope assumes that the two sources to resolve are of equal brightness. For a planet and its host star, the contrast, which is the ratio of the stellar flux over the planetary flux, ranges from 10^4 for close-in hot planets to 10^{10} for cold distant ones. At such contrasts (above 10^4), the photo-noise produced by the secondary lobs of the PSF, which contain 16% of the total energy for an ideal Airy disc PSF, is enough to drown the planetary signal. For this reason, DI is more suited to observe hot and thus young giant planets that are still radiating their accretion energy. Planets that are kept hot by the stellar insulation are indeed out of reach due to insufficient angular resolution.

In any case, DI relies on coronagraphs to reduce the contrast by suppressing the stellar light while preserving the planetary signal. The simplest optical concept for a coronagraph still commonly used is called classical Lyot coronagraph (Lyot, 1932). It consists in a circular occulting mask positioned on the line of sight, in the image plane, which obstructs the stellar light while leaving the light from the surrounding intact. Other concepts exist: apodized Lyot coronagraph (Aime, Soummer, & Ferrari, 2002), 4 quadrants phase mask (Rouan, Riaud, Boccaletti, Clénet, & Labeyrie, 2000), Vortex (Mawet, Riaud, Absil, & Surdej, 2005; Foo, Palacios, & Swartzlander, 2005). The performances of a coronagraph are quantified by the properties of its search area; The angular domain in which a planet can be detected. Several properties of the search area can be used (see Guyon, Pluzhnik, Kuchner, Collins, & Ridgway, 2006, for more details). The most common ones are its throughput (it can range from 10 to 100%) and its inner working angle (the angular separation at which the throughput for the planet is half of the maximal throughput—it can range from 0.5 to $4\lambda/D$).

Diffraction and optical defects on the optical path leading to the coronagraph scatter the stellar light away from the line of sight and produces speckles in the search area. To mitigate these speckles and maximise the signal-to-noise ratio, several post processing techniques called differential imaging techniques have been developed. The most common ones are angular differential imaging (ADI, Marois, Lafrenière, Doyon, Macintosh, & Nadeau, 2006) and spectral differential imaging (SDI, Marois, Doyon, Racine, & Nadeau, 2000; Racine, Walker, Nadeau, Doyon, & Marois, 1999). Speckles are mostly due to diffraction of the stellar light by imperfection of the optical surfaces. Their spatial distribution and size scales with the wavelength of observation while the location of the planet on the image doesn't. The SDI technique thus relies on two images taken simultaneously at two different but adjacent wavelengths to correct for the speckles while preserving the planetary signal. In practice, the image taken at the shorter wavelength is spatially dilated by the ratio of the wavelengths. The intensity in the two images are then normalized. Finally, one is subtracted by the other. As a result, the speckles signal is significantly reduced while the planet appears as a positive pic adjacent to a negative pic. The other differential imaging technique commonly used, ADI,

relies on the variation of the parallactic angle during an observation sequence. When the field de-rotator is deactivated on an alt-azimuthal telescope mount, the location of the planet rotates with the parallactic angle, while the stellar speckles stay comparatively constant due to the location of the star on the line of sight. The ADI method thus uses images taken at different parallactic angles to create a high signal-to-noise ratio templates of the stellar speckles that can be subtracted to the individual images without subtracting the planetary signal. When the instrument allows it, ADI can be used after SDI to correct for differential aberration between wavelengths and further improve the signal-to-noise. The reader interested in more details on differential imaging techniques (for example reference differential imaging, polarimetric differential imaging, coherent differential imaging) or on PSF calibration techniques can refer to (Chauvin, 2018).

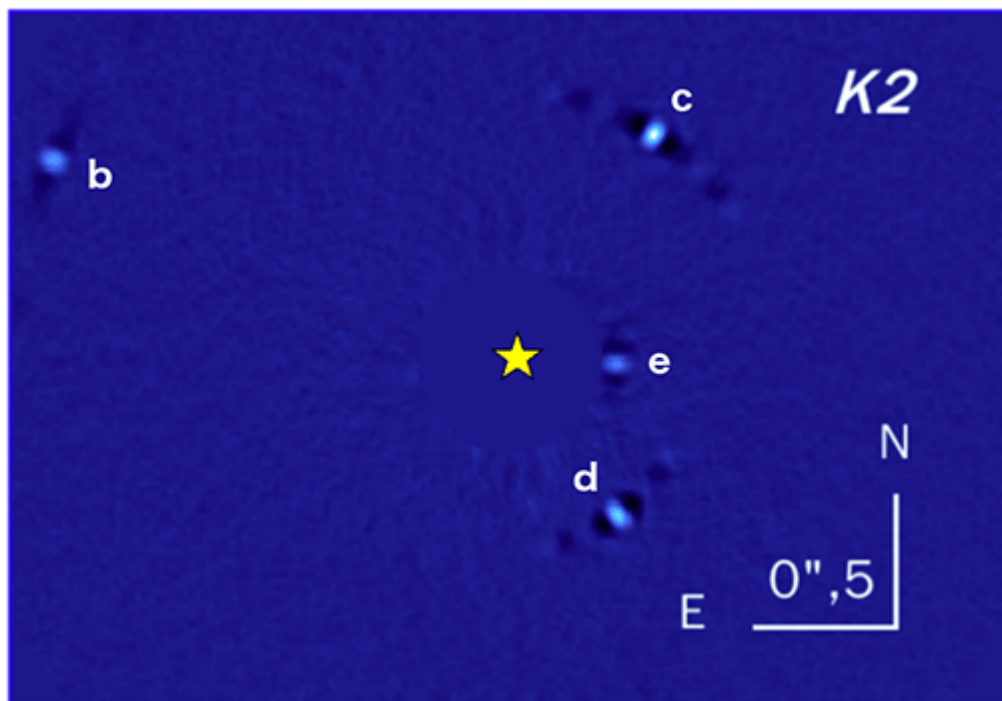


Figure 6. Direct imaging observation of the HR 8799 system by the SPHERE-IRDIS in the K2 band (around $2.25\mu\text{m}$). These observations reduced using the angular differential imaging technique and clearly exhibit the 4 planets in this system. The yellow star symbol indicates the position of central star. The letters next to the 4 planetary signals visible in this image give the name of these planets. Figure based on Zurlo et al. (2016).

Even if DI is less prolific than transit and radial velocity in terms of number of detected planets, it is a very promising technique for atmosphere characterization of an Earth like planet in the habitable zone of its parent star. Furthermore, it has already produced emblematic detections like β Pictoris b (Lagrange et al., 2010), the HR 8799 planetary system (Marois et al., 2008) — see Figure 6 — or 51 Eri b (Macintosh et al., 2015). The technique has also proven to be highly valuable for the observation of proto-planetary disc and to decipher planetary formation processes (see for example the observations of the disc around MWC 758, Benisty et al., 2015).

Microlensing

The concept of gravitational lens originates from Einstein's theory of general relativity (Einstein, 1916). It predicts that mass alters the curvature of space and time and as a result can curve the trajectory of a photon. In 1936, Einstein (Einstein, 1936) predicted that a foreground star can displace the apparent position of a background star as an optical lens changes the apparent position of object observed through it. Like an optical lens, in favorable geometrical conditions, a star can also focus the light from the background star toward us, observers, and thus enhance its apparent magnitude.

Several decades later, the theory was extended to describe the gravitational lensing produced by binary stars or a star-planet system (Gould & Loeb, 1992; Mao & Paczynski, 1991).

Microlensing as a planet detection method refers to the additional magnification lensing event produced by a planet during the magnification lensing event generated by its host star. Stars' and planets' magnification events are called microlensing as opposed to the comparatively much larger magnification that galaxies as lenses can produce.

Due to the analogy with optical lenses, the foreground star is traditionally called the lens and the background star is called the source. When the source, the lens, and the observer are perfectly aligned, the observer sees the source as a ring of light surrounding the lens. This ring is called the Einstein ring. Its angular size is given by

$$\theta_E = \sqrt{\frac{4G}{c^2} M_L \frac{D_S - D_L}{D_S D_L}}, \quad (15)$$

where c is the speed of light, G is the gravitation constant, D_S is the distance between the observer and the source, D_L is the distance between the observer and the lens and M_L is the mass of the lens. If the source, the lens, and the observer are not aligned, a microlensing event is observed only when the angular separation between the source and the lens is close to or lower than θ_E . In this case, the observer can see up to two stretched images of the source. They are called the major and minor images and are located outside and inside of the Einstein ring respectively. Their respective angular position (θ_+ and θ_-) and source magnification factor (A_+ and A_-) are given by:

$$\frac{\theta_{\pm}}{\theta_E} = \pm \frac{\sqrt{u^2 + 4} \pm u}{2} \quad (16)$$

$$A_{\pm} = \frac{1}{2} \left(\frac{u^2 + 2}{u\sqrt{u^2 + 4}} \pm 1 \right), \quad (17)$$

where $u = \frac{\beta}{\theta_E}$ is the ratio of the real angular position of the source with respect to lens over the radius of the Einstein ring.

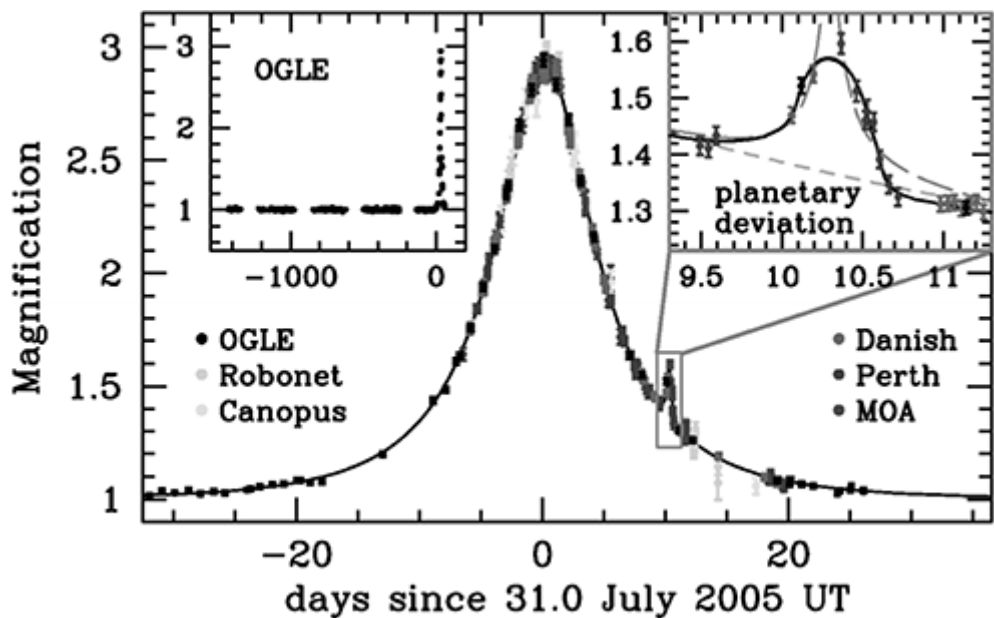


Figure 7. Microlensing event from the OGLE-2005-BLG-390 planetary system: An M-dwarf star and a $5.5 M_{\oplus}$ super-Earth planet. The light-curve is a combination of data from several instruments: PLANET Danish (ESO La Silla, red points), PLANET Perth (blue), PLANET Canopus (Hobart, cyan), RoboNet Faulkes North (Hawaii, green), OGLE (Las Campanas, black), MOA (Mt John Observatory, brown). A zoom on the microlensing event produced by the planet is shown in the top left inset. The dashed grey curve is the best binary source model, while the dashed orange line is the best single lens model (both rejected by the data). The black line is the best star-planet lens model. From Beaulieu et al. (2006).

The equations for a star-planet system are more complex (see for example Batista, 2018), but as a first order approximation, the dependence of the amplification factor with θ_E and thus with $\sqrt{M_{pl}}$, the square root of the planet mass, remains. Consequently, microlensing is relatively more sensitive to low mass planets than other detection methods. However, it has one important drawback: the difficulty to re-observe the same planetary system. The configuration leading to a microlensing event is quite rare, around one in a million for the galactic bulge where the density of foreground and background stars is the highest. Compared with the $\sim 10^7$ stars in the galactic bulge, the probability of microlensing events is not so low. However, it is very unlikely that the same star-planet system observed thanks to a micro lensing event produces an additional microlensing event with another background star.

Some of the most emblematic detections made with the microlensing technique are OGLE-2003-BLG-235Lb/MOA-2003-BLG-53b (Bond et al., 2004), the first planet detected with microlensing, OGLE-2005-BLG-390Lb (Beaulieu et al., 2006), the first super-Earth (see Figure 7), and OGLE-2006-BLG-109Lb,c (Bennett et al., 2010; Gaudi et al., 2008), the first multi-planetary system.¹¹

Detecting Atmospheres

Among the few ways that are considered viable for the search of life outside of the solar system, the detection of bio-signatures in the atmosphere of a rocky planet is indubitably the most explored (e.g., Des Marais et al., 2002). There is still a long way before the technology required to detect bio-signatures in the atmosphere of an Earth-like planet orbiting a Sun-like star is ready. However, there is a lot of interesting science and technological developments to be done along the way.

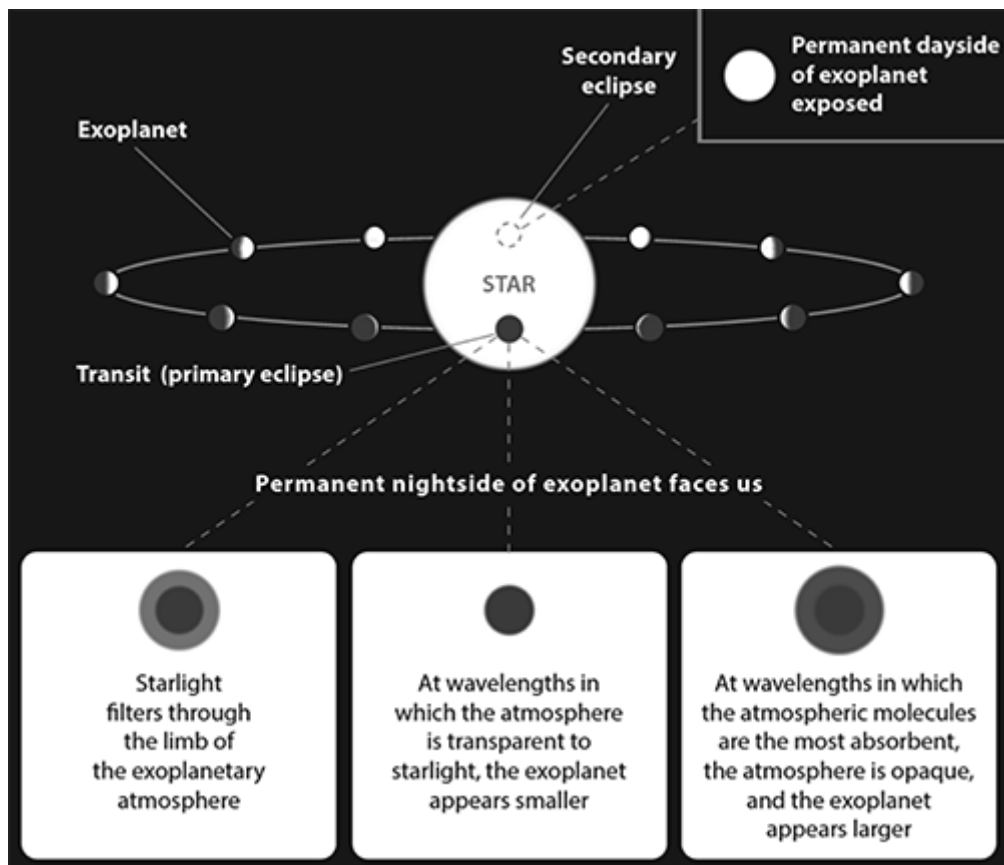


Figure 8. Information from exoplanet atmosphere can be obtained from transit, occultation, and phase-curves.

Figure extracted from Heng and Showman (2015)

Transmission Spectroscopy

Most of the instruments capable of detecting and studying the properties of exoplanetary atmospheres rely on technologies originally designed to detect exoplanets. The first technique is transit spectroscopy. As the name suggests, it is inspired from the transit photometry technique. When analysing transit photometry data, one usually assumes that the planet is an optically opaque sphere with a fixed radius. But if one considers a planet with a gaseous atmosphere, the notion of radius is not completely clear. The transmission of the atmosphere varies from transparent to opaque towards the centre (see Figure 8). The radius at which the planetary atmosphere becomes opaque depends on the wavelength of observation and on the characteristics of the atmosphere (composition, density, particle size). The transit depth is thus wavelength dependent and can be expressed as

$$\begin{aligned}
\frac{\Delta L}{L}(\lambda) &= \left(\frac{R_{p,\text{eff}}(\lambda)}{R_{\text{star}}} \right)^2 \\
&= \left(\frac{R_p}{R_{\text{star}}} \right)^2 + \frac{2R_p \delta R_p(\lambda)}{R_{\text{star}}^2} \\
&\sim \left(\frac{R_p}{R_{\text{star}}} \right)^2 + \frac{2R_p}{R_{\text{star}}^2} \alpha(\lambda) \left(5 \frac{kT}{\mu g} \right).
\end{aligned} \tag{18}$$

Each line of these equations represents a different level of complexity in the description of the variation of the transit depth with wavelength. In the first line, $R_{p,\text{eff}}(\lambda)$ is called the effective radius of the planet at the wavelength λ . It is the equivalent radius that an opaque sphere needs to have to produce the depth of the transit observed at this wavelength. In the second line, the first term is associated to the radius up to which the planet is completely opaque at all wavelengths (R_p). The second term is associated to the extra opaque annulus of height δR_p , which is required to explain the transit depth observed at a given wavelength. Finally, in the third line, $\delta R_p(\lambda)$ is approximated by 5 times the atmospheric scale height (H) multiplied by a factor, $\alpha(\lambda)$, describing the spectral variation of transparency of the annulus— $\alpha(\lambda)$ is close to unity. The scale height is the height, from the planetary surface (in our case R_p), at which one needs to raise for the pressure to drop by a factor $1/e$ in an isothermal atmosphere under hydrostatic equilibrium. The scale height is given by $H = (kT)/(\mu g)$ where k is the Boltzmann's constant, T is the atmospheric temperature, μ is the mean molecular weight and g is the gravity at the surface of the planet.

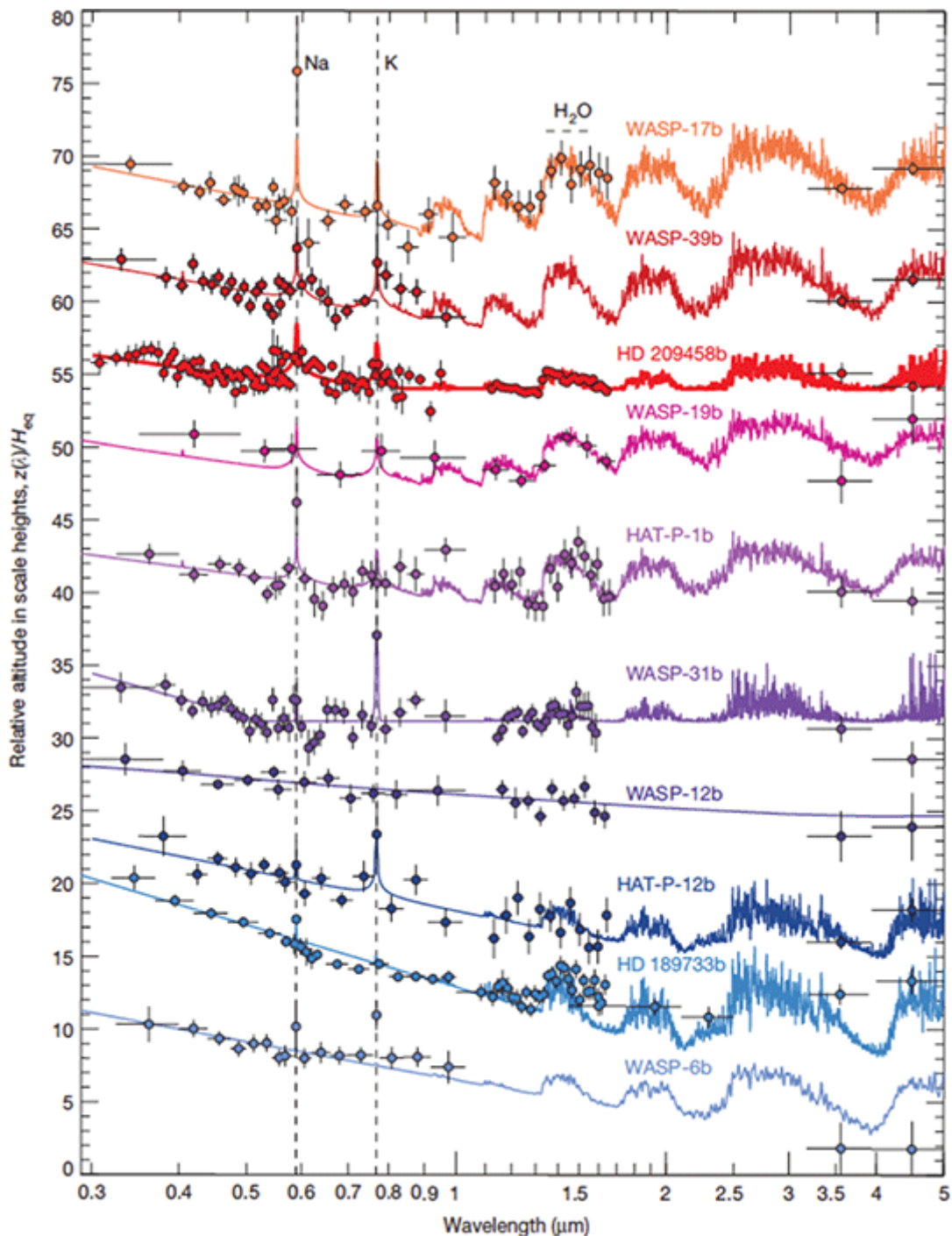


Figure 9. Sample of exoplanet transmission spectra obtained with the transit spectroscopy. To enable a comparison between exoplanets with different scale heights (H), the transmission spectrum is expressed in relative altitude in scale height. It corresponds to the effective radius measured at a given wavelength divided by the scale height. The points correspond to the data collected with WFC3@HST and IRAC@Spitzer and the solid lines correspond to best fit atmospheric models for each planet. An offset is added to the spectra for visualization purpose. This sample illustrates the continuum from clear (top) to hazy and cloudy (bottom) atmospheres.

Figure extracted from Sing et al. (2016)

By measuring transits in different wavelength bins, one can thus measure $R_{p,\text{eff}}(\lambda)$ and infer $\alpha(\lambda)$, which reflects the size of the particles that compose the atmosphere and its molecular and atomic composition (see Fig. 9). The amplitude of these wavelength dependent variations are of the order of 100 ppm in the most favorable cases, hot giant planets around a G type star. In the case of a Earth-radius planet, the amplitude of the variation is around 0.1 to 1 ppm, depending on the host star. These observations thus requires both spectral resolution and photometric precision.

The first observations of this kind where made with the HST-STIS instrument during a transit of HD209458 b (Charbonneau, Brown, Noyes, & Gilliland, 2002) and resulted in the clear detection of Sodium in the atmosphere of this planet. These kinds of observations are more challenging from the ground. The Earth atmosphere induces a decrease in photometric precision but more importantly wavelength dependant systematic trends. The later can be mitigated by the observation of comparison stars simultaneously to the observation of the target as for the observation of WASP-49 b with the VLT-FORS2 instrument (Lendl et al., 2016). Alternatively, because they are designed to avoid or calibrate spectral variations induced by the atmosphere and preserve spectral lines profiles in order to achieve high radial velocity precision, highly stabilized fiber-fed high resolution spectrograph can compensate their lack of photometric precision and be used for transit spectroscopy. The analysis of the observation of 3 transits of HD189733 b (Wytttenbach, Ehrenreich, Lovis, Udry, & Pepe, 2015) has demonstrated that HARPS was able to measure the change of depth and shape, induced by the absorption the stellar light by Sodium.

Secondary Eclipses

Transit spectroscopy is not the only available tool to detect and characterize exoplanet atmospheres. Using high precision photometry, the light emitted or reflected by the planet can be disentangled from the stellar light due its correlation with the orbital phase of the planet. The first demonstration of this principle is the observation of planetary secondary eclipse (also called occultation). The high precision photometric observation of a planet passing behind its parents star yield a transit like feature as observed for HD198733 b by IRAC-Spitzer (Knutson et al., 2007). In the infra-red, where the thermal emission is the highest, secondary eclipses reflect the temperature of the day-side of the planet (e.g., Koll et al., 2019). In the visible, where the stellar light reflected by the planet is at its peak, the geometric albedo can be inferred.

Phase-Curves

The observations, in the infra-red, of HD198733 b by IRAC-Spitzer (Knutson et al., 2007) revealed more than the temperature of its day-side. The continuous monitoring of the photometry of this star-planet system, between transit and occultation, displays a continuous increase of light intensity produced by the changes of planetary phases called phase-curve. Strong tides exerted by the star on the planet due to their proximity induce a synchronization between rotation of the planet and its orbital motion. Consequently, the same hemisphere of the planet always faces the star, while the other hemisphere never sees direct stellar light. When the planet transits, we, as observers, are facing its night-side. During its journey from

transit to occultation, the portion of the planetary surface that we are seeing, as observers, slowly rotates from night-side to day-side and produces the phase-curve signal observed by IRAC-Spitzer. The analysis of phase-curves delivers the longitudinal brightness map of the planetary surface which is a tell-tale of the energy redistribution processes over the planetary surface (such as winds). As for transits, occultation and phase-curves observed at different wavelength can deliver a wealth of information. The spectroscopic phase-curve of WASP-43 b measured by WFC3-HST (Stevenson et al., 2014) provided evidence of the presence of water vapor on the day-side of the planet. The infrared ($4.5\mu\text{m}$) phase curve of the exoplanet LHS 3844b allowed measurement of the temperature map of a terrestrial exoplanet and rule out the presence of a thick atmosphere (Kreidberg et al., 2019), see Figure 10.

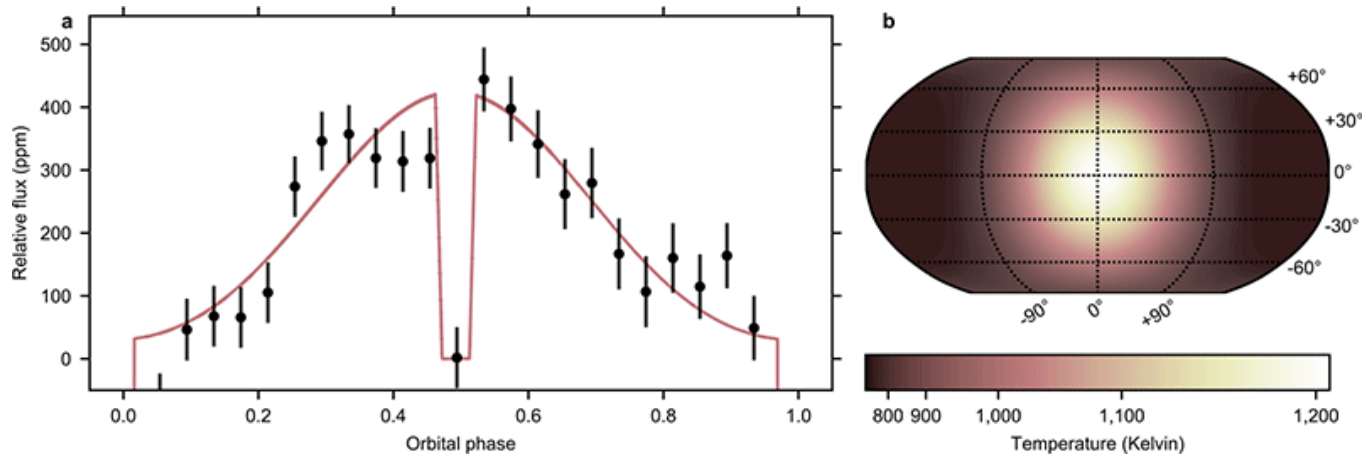


Figure 10. *Left:* Phase curve of the terrestrial planet LHS 3844 b measured with IRAC@Spitzer (Fazio et al., 2004). The red line is the best fit model. The black dots are the binned observations with their 1σ error bars. *Right:* Best fit temperature map corresponding to the observed phase curve. We note that the phase-curve only allows to constrain the longitudinal variations. The latitudinal variations displayed here are not constrained by the data. They are solely a consequence of the model used, which is based on spherical harmonics.

Figure extracted from Kreidberg et al. (2019)

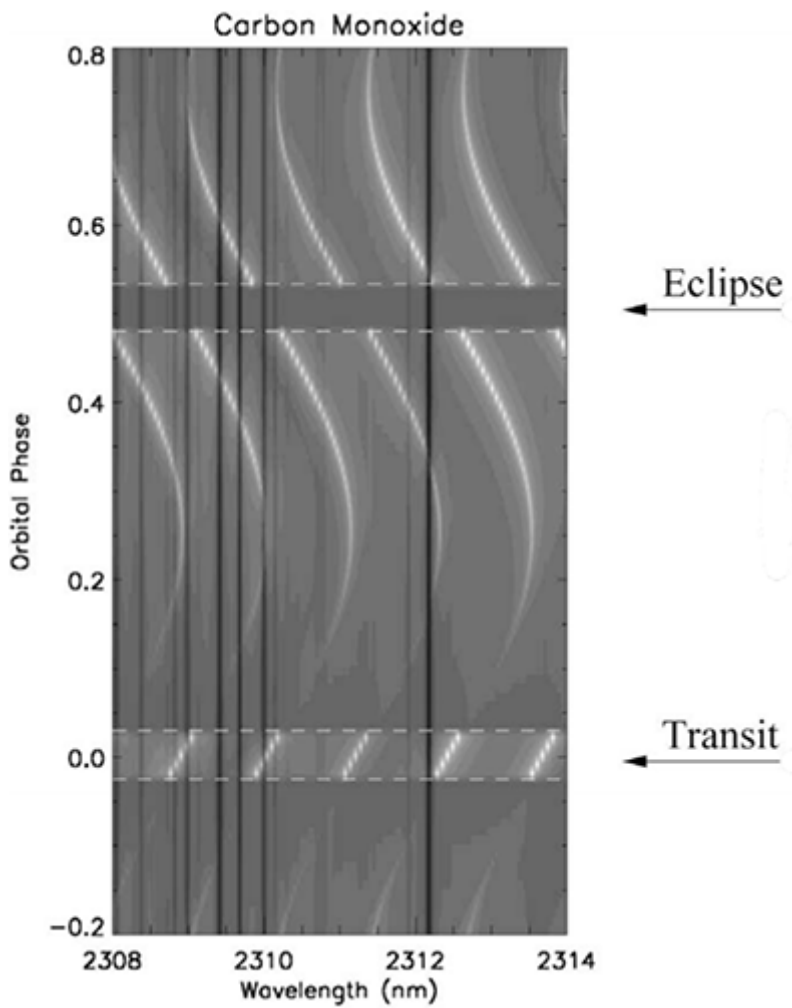


Figure 11. Simulations of the phase-curve of HD209458 b observed at high spectroscopic resolution by CRIRES. The simulation focus here on the region between 2.29 and 2.34 μm containing absorption lines of CO. These lines, shown in white for visualization purpose, follow a sinusoidal pattern with orbital phase due to the doppler shift produced by the orbital motion of the planet. The vertical dark lines are telluric absorption lines.

Figure extracted from Snellen et al. (2010a).

Correlation with the orbital phases of the planet has also been used in combination with high resolution spectroscopy to disentangle the stellar and planetary light. The first detection of this kind was made on HD209458 b in the near-infrared with CRIRES (Snellen et al., 2010b)—Figure 11. The cross correlation of the spectra taken during 5 hours around the transit with a template spectrum of CO provided a shallow hint of the presence of these planetary absorption lines. By taking into account the Doppler shift of these lines due to the planetary motion, the signals contained in each individual spectrum could be coherently summed. A significant detection was only possible thanks to the correlation of the signal with the planetary orbital phases. A similar methodology was also used to detect the stellar absorption lines reflected by the planet 51Peg b (Martins et al., 2015) with HARPS in the visible. Once again, the correlation of the signal with the orbital phases was fundamental to increase the signal-to-noise ratio of the detection.

Direct Imaging

Direct imaging is likely the most challenging, but also the most intuitive way to characterize the atmosphere of a planet. As planet and star are angularly resolved, direct imaging observations at different wavelength deliver a integrated spectrum of the atmosphere of the planet. Striking examples are the spectra of the planets in the HR8799 system. The detection of the CO and water vapor in the atmosphere of HR8799c with the OSIRIS-Keck spectrograph (Konopacky, Barman, Macintosh, & Marois, 2013) and later the spectra of HR8799d are obtained with SPHERE-VLT (Zurlo et al., 2016).

Conclusions and Prospects

Thanks to the development of precise ground and space based instrumentation, together with our understanding of noise sources and data analysis methods, the detection and characterization of exoplanets is done on a routine basis. Less than three decades after the discovery of the first exoplanet orbiting a solar-type star, we know that planets are ubiquitous in our Galaxy, rocky planets being the most common. Although no real Earth analogue has yet been discovered, the prospects for such a detection are extremely positive.

In the next few years, the exoplanet community will have access to an array of instruments that will allow the study of entire planetary systems around nearby bright stars. The legacy of Kepler in the search for transits of small planets will be in the hands of projects and missions such as the Next Generation Transit Search (NGTS; Wheatley et al., 2013), the MEarth project (Irwin, Charbonneau, Nutzman, Falco, & Stempels, 2009), and the TESS (Ricker et al., 2016), CHEOPS (Broeg et al., 2013) and PLATO2.0 (Rauer et al., 2014) space missions. Radial-velocity surveys will continue to explore planetary systems in the solar neighborhood, with high-precision spectrographs like HARPS, HARPS-N, Keck/HIRES and APF/Lick, as well as upcoming instruments such as HARPS-3. The cm/s level is on sight with ESPRESSO (Pepe et al., 2014), and the NIR domain is open for exploration with CARMENES/Calar Alto (Quirrenbach et al., 2010), SPiROU/CFHT (Artigau et al., 2014), HPF/HET (Mahadevan et al., 2010), GIANO/TNG (Oliva et al., 2004), and NIRPS (Wildi et al., 2017). Follow-up of transit detections with these instruments will provide precise densities and internal compositions for a large number of planets.

The Gaia mission already started delivering high-accuracy fundamental stellar parameters for all the planet host stars (Lindegren et al., 2016) and will also detect giant planets at intermediate semi-major axes. The James Webb Space Telescope (Gardner et al., 2006), the Ariel mission (Tinetti et al., 2016), and future ground-based extremely large telescopes with their instrumentation sets (e.g., HIRES@ELT Marconi et al., 2018) will study the atmospheric composition of the planets with both transmission and emission spectroscopy. In brief, the instrumentation of the next few years will answer many of the most important questions about exoplanets. Many other new surprises will come as new discoveries arise. It may very well be that one of these instruments or missions will be the first to discover the first Earth-like planet orbiting another Sun.

Acknowledgments

This work was supported by FCT - Fundação para a Ciência e a Tecnologia through national funds and by FEDER through COMPETE2020 - Programa Operacional Competitividade e Internacionalização by these grants: UID/FIS/04434/2019; UIDB/04434/2020; UIDP/04434/2020; PTDC/FIS-AST/32113/2017 & POCI-01-0145-FEDER-032113; PTDC/FIS-AST/28953/2017 & POCI-01-0145-FEDER-028953. O.D. and J.P.F. are supported in the form of work contracts funded by national funds through FCT with references DL57/2016/CP1364/CT0004 and DL57/2016/CP1364/CT0005. SCCB also acknowledges support from FCT through Investigador FCT contracts IF/01312/2014/CP1215/CT0004.

References

- Agol, E., Luger, R., & Foreman-Mackey, D. (2020). Analytic planetary transit light curves and derivatives for stars with polynomial limb darkening. *Astronomical Journal*, 159(3), 123.
- Aigrain, S., Hodgkin, S. d T., Irwin, M. J., Lewis, J. R., & Roberts, S. J. (2015). Precise time series photometry for the Kepler-2.0 mission. *MNRAS*, 447(3), 2880–2893.
- Aime, C., Soummer, R., & Ferrari, A. (2002). Total coronagraphic extinction of rectangular apertures using linear prolate apodizations. *Astronomy and Astrophysics*, 389(1), 334–344.
- Airy, G. B. (1838). On the Intensity of Light in the neighbourhood of a caustic. *Transactions of the Cambridge Philosophical Society*, 6, 379.
- Albrecht, S., Winn, J. N., Johnson, J. A., Howard, A. W., Marcy, G. W., Butler, R. P., . . . Hartman, J. D. (2012). Obliquities of hot Jupiter host stars: Evidence for tidal interactions and primordial misalignments. *Astrophysical Journal*, 757(1), 18.
- Anglada-Escudé, G., Amado, P. J., Barnes, J., Berdiñas, Z. M., Butler, R. P., Coleman, G. A. L., . . . Zechmeister, M. (2016). A terrestrial planet candidate in a temperate orbit around Proxima Centauri. *Nature*, 536(7617), 437–440.
- Anglada-Escudé, G., Tuomi, M., Gerlach, E., Barnes, R., Heller, R., Jenkins, J. S., . . . Jones, H. R. A. (2013). A dynamically packed planetary system around GJ 667C with three super-Earths in its habitable zone. *Astronomy & Astrophysics*, 556, A126.
- Armstrong, D. J., Pollacco, D., & Santerne, A. (2017). Transit shapes and self-organizing maps as a tool for ranking planetary candidates: Application to Kepler and K2. *Monthly Notices of the Royal Astronomical Society*, 465, 2634–2642.
- Artigau, E., Kouach, D., Donati, J.-F., Doyon, R., Delfosse, X., Baratchart, S., . . . Figueira, P. (2014). SPIRou: The near-infrared spectropolarimeter/high-precision velocimeter for the Canada-France-Hawaii telescope. *Proceedings SPIE 914715: Ground-Based and Airborne Instrumentation for Astronomy V*.
- Astudillo-Defru, N., Díaz, R. F., Bonfils, X., Almenara, J. M., Delisle, J. B., Bouchy, F., . . . Wünsche, A. (2017). The HARPS search for southern extra-solar planets. XLII. A system of Earth-mass planets around the nearby M dwarf YZ Ceti. *Astronomy & Astrophysics*, 605, L11.
- Baluev, R. V. (2013). The impact of red noise in radial velocity planet searches: Only three planets orbiting GJ 581? *Monthly Notices of the Royal Astronomical Society*, 429(3), 2052–2068.

Baluev, R. V. & Shaidulin, V. S. (2015). Analytic models of the Rossiter-McLaughlin effect for arbitrary eclipses/star size ratios and arbitrary multiline stellar spectra. *Monthly Notices of the Royal Astronomical Society*, 454(4), 4379–4399.

Baraffe, I., Chabrier, G., & Barman, T. (2008). Structure and evolution of super-Earth to super-Jupiter exoplanets. I. Heavy element enrichment in the interior. *Astronomy & Astrophysics*, 482(1), 315–332.

Baranne, A., Queloz, D., Mayor, M., Adrianzyk, G., Knispel, G., Kohler, D., . . . & Vin, A. (1996). ELODIE: A spectrograph for accurate radial velocity measurements. *Astronomy and Astrophysics Supplement Series*, 119(2), 373–390.

Barclay, T., Endl, M., Huber, D., Foreman-Mackey, D., Cochran, W. D., MacQueen, P. J., . . . Quintana, E. V. (2015). Radial velocity observations and light curve noise modeling confirm that Kepler-91b is a giant planet orbiting a giant star. *Astrophysical Journal*, 800(1), 46.

Barros, S. C. C., Almenara, J. M., Deleuil, M., Diaz, R. F., Csizmadia, S., Cabrera, J., . . . Wuchterl, G. (2014). Revisiting the transits of CoRoT-7b at a lower activity level. *Astronomy & Astrophysics*, 569, A74.

Barros, S. C. C., Boué, G., Gibson, N. P., Pollacco, D. L., Santerne, A., Keenan, F. P., . . . Street, R. A. (2013). Transit timing variations in WASP-10b induced by stellar activity. *Monthly Notices of the Royal Astronomical Society*, 430(4), 3032–3047.

Barros, S. C. C., Demangeon, O., & Deleuil, M. (2016). New planetary and eclipsing binary candidates from campaigns 1–6 of the K2 mission. *Astronomy & Astrophysics*, 594, A100.

Barros, S. C. C., Gosselin, H., Lillo-Box, J., Bayliss, D., Delgado Mena, E., Brugger, B., . . . Wyttenbach, A. (2017). Precise masses for the transiting planetary system HD 106315 with HARPS. *Astronomy & Astrophysics*, 60, A25.

Batalha, N. M., Rowe, J. F., Bryson, S. T., Barclay, T., Burke, C. J., Caldwell, D. A., . . . Welsh, W. F. (2013). Planetary candidates observed by Kepler: III, Analysis of the first 16 months of data. *Astrophysical Journal Supplement Series*, 204(2), 24.

Batista, V. (2018). Finding planets via gravitational microlensing. In J. Deeg & J. A. Belmonte (Eds.), *Handbook of Exoplanets* (pp. 659–687). Cham, Switzerland: Springer International.

Beaulieu, J.-P., Bennett, D. P., Fouqué, P., Williams, A., Dominik, M., Jørgensen, U. G., . . . Yoshioka, T. (2006). Discovery of a cool planet of 5.5 Earth masses through gravitational microlensing. *Nature*, 439(7075), 437–440.

Belorizky, D. (1938). Le Soleil, étoile variable. *L'Astronomie*, 52, 359–361.

Benedict, G. F., McArthur, B. E., Gatewood, G., Nelan, E., Cochran, W. D., Hatzes, A., . . . Paulson, D. B. (2006). The extrasolar planet Eridani b: Orbit and mass. *Astronomical Journal*, 132(5), 2206.

Benisty, M., Juhasz, A., Boccaletti, A., Avenhaus, H., Milli, J., Thalmann, C., . . . Pueyo, L. (2015). Asymmetric features in the protoplanetary disk MWC 758. *Astronomy and Astrophysics*, 578, L6.

- Bennett, D. P., Rhie, S. H., Nikolaev, S., Gaudi, B. S., Udalski, A., Gould, A., . . . Frank, S. (2010). Masses and orbital constraints for the OGLE-2006-BLG-109Lb,c Jupiter/Saturn analog planetary system. *Astrophysical Journal*, 713(2), 837.
- Boisse, I., Moutou, C., Vidal-Madjar, A., Bouchy, F., Pont, F., Hébrard, G., . . . Udry, S. (2009). Stellar activity of planetary host star HD 189 733. *Astronomy and Astrophysics*, 495, 959–966.
- Bond, I. A., Udalski, A., Jaroszyński, M., Rattenbury, N. J., Paczyński, B., Soszyński, I., . . . Zebrun, K. (2004). OGLE 2003-BLG- 235/MOA 2003-BLG-53: A planetary microlensing event. *Astrophysical Journal*, 606(2), L155.
- Bonfils, X., Astudillo-Defru, N., Díaz, R., Almenara, J. M., Forveille, T., Bouchy, F., . . . Wünsche, A. (2018). A temperate exo-Earth around a quiet M dwarf at 3.4 parsec. *Astronomy and Astrophysics*, 613, A25.
- Bonfils, X., Delfosse, X., Udry, S., Forveille, T., Mayor, M., Perrier, C., . . . Bertaux, J.-L. (2013). The HARPS search for southern extra-solar planets: XXXI. The M-dwarf sample. *Astronomy and Astrophysics*, 549, A109.
- Bonfils, X., Mayor, M., Delfosse, X., Forveille, T., Gillon, M., Perrier, C., . . . Bertaux, J.-L. (2007). The HARPS search for southern extra-solar planets. X. A $m \sin i = 11$ M Earth planet around the nearby spotted M dwarf GJ674. *Astronomy and Astrophysics*, 474(1), 293–299.
- Borucki, W. J., Koch, D. G., Basri, G., Batalha, N., Brown, T. M., Bryson, S. T., . . . Still, M. (2011). Characteristics of planetary candidates observed by Kepler. II. Analysis of the first four months of data. *Astrophysical Journal*, 736(1), 19.
- Broeg, C., Fortier, A., Ehrenreich, D., Alibert, Y., Baumjohann, W., Benz, W., . . . the CHEOPS team (2013). *CHEOPS: A transit photometry mission for ESA's small mission programme* <<https://doi.org/10.1051/epjconf/20134703005>>. EPJ Web of Conferences, 47, 03005.
- Brogi, M., Snellen, I. A. G., de Kok, R. J., Albrecht, S., Birkby, J., & de Mooij, E. J. W. (2012). The signature of orbital motion from the dayside of the planet τ Bootis b. *Nature*, 486(7404), 502–504.
- Burke, C. J., Mullally, F., Thompson, S. E., Coughlin, J. L., & Rowe, J. F. (2019). Re-evaluating small long-period confirmed planets from Kepler. *Astrophysical Journal*, 157(4), 143.
- Burrows, A. S. (2014). Highlights in the study of exoplanet atmospheres. *Nature*, 513(7518), 345–352.
- Butler, R. P., & Marcy, G. W. (1996). A planet orbiting 47 Ursae Majoris. *Astrophysical Journal*, 464(2), L153.
- Butler, R. P., Marcy, G. W., Fischer, D. A., Brown, T. M., Contos, A. R., Korzennik, S. G., . . . Noyes, R. W. (1999). Evidence for multiple companions to u Andromedae. *Astrophysical Journal*, 526(2), 916.
- Butler, R. P., Vogt, S. S., Marcy, G. W., Fischer, D. A., Wright, J. T., Henry, G. W., . . . Lissauer, J. J. (2004). A Neptune-mass planet orbiting the nearby M dwarf GJ 436. *Astrophysical Journal*, 617(1), 580.

-
- Campbell, B., Walker, G. A. H., & Yang, S. (1988). A search for substellar companions to solar-type stars. *Astrophysical Journal*, 331, 902–921.
- Carter, J. A., Agol, E., Chaplin, W. J., Basu, S., Bedding, T. R., Buchhave, L. A., . . . Winn, J. N. (2012). Kepler-36: A pair of planets with neighboring orbits and dissimilar densities. *Science*, 337, 556–559.
- Cegla, H. M., Watson, C. A., Shelyag, S., Mathioudakis, M., & Moutari, S. (2019). Stellar surface magnetoconvection as a source of astrophysical noise. III: Sun-as-a-star simulations and optimal noise diagnostics. *Astrophysical Journal*, 879(1), 55.
- Charbonneau, D., Brown, T. M., Latham, D. W., & Mayor, M. (2000). Detection of planetary transits across a sun-like star. *Astrophysical Journal*, 529(1), L45.
- Charbonneau, D., Brown, T. M., Noyes, R. W., & Gilliland, R. L. (2002). Detection of an extrasolar planet atmosphere. *The Astrophysical Journal*, 568(1), 377.
- Chauvin, G. (2018). Direct imaging of exoplanets at the era of the extremely large telescopes. *arXiv e-prints*. arXiv:1810.02031.
- Cloutier, R., Astudillo-Defru, N., Doyon, R., Bonfils, X., Almenara, J. M., Benneke, B., . . . Wünsche, A. (2017). Characterization of the K2-18 multiplanetary system with HARPS. A habitable zone super-Earth and discovery of a second, warm super-Earth on a non-coplanar orbit. *Astronomy and Astrophysics*, 608, A35.
- Cloutier, R., Astudillo-Defru, N., Doyon, R., Bonfils, X., Almenara, J.-M., Bouchy, F., . . . Wünsche, A. (2019). Confirmation of the radial velocity super-Earth K2-18c with HARPS and CARMENES. *Astronomy and Astrophysics*, 621, A49.
- Correia, A. C. M., Couetdic, J., Laskar, J., Bonfils, X., Mayor, M., Bertaux, J.-L., . . . Udry, S. (2010). The HARPS search for southern extra-solar planets: XIX. Characterization and dynamics of the GJ 876 planetary system. *Astronomy and Astrophysics*, 511, A21.
- Damasso, M., & Sordo, F. D. (2017). Proxima Centauri reloaded: Unravelling the stellar noise in radial velocities. *Astronomy & Astrophysics*, 599, A126.
- Dawson, R. I., & Johnson, J. A. (2018). Origins of hot Jupiters. Annual Review of Astronomy and Astrophysics, 56, 175–221.
- Delfosse, X., Forveille, T., Mayor, M., Perrier, C., Naef, D., & Queloz, D. (1998). The closest extrasolar planet. A giant planet around the M4 dwarf GL 876. *Astronomy & Astrophysics*, 338, L67–L70.
- Delisle, J.-B., Ségransan, D., Dumusque, X., Diaz, R. F., Bouchy, F., Lovis, C., . . . Wyttenbach, A. (2018). The HARPS search for southern extra-solar planets—XLIII. A compact system of four super-Earth planets orbiting HD 215152. *Astronomy & Astrophysics*, 614, A133.
- Des Marais, D. J., Harwit, M. O., Jucks, K. W., Kasting, J. F., Lin, D. N. C., Lunine, J. I., . . . Woolf, N. J. (2002). Remote sensing of planetary properties and biosignatures on extrasolar terrestrial planets. *Astrobiology*, 2, 153.

-
- Desort, M., Lagrange, A.-M., Galland, F., Udry, S., & Mayor, M. (2007). Search for exoplanets with the radial-velocity technique: Quantitative diagnostics of stellar activity. *Astronomy & Astrophysics*, 473, 983–993.
- Díaz, R. F., Almenara, J. M., Santerne, A., Moutou, C., Lethuillier, A., & Deleuil, M. (2014). PASTIS: Bayesian extrasolar planet validation—I: General framework, models, and performance. *Monthly Notices of the Royal Astronomical Society*, 441(2), 983–1004.
- Díaz, R. F., Ségransan, D., Udry, S., Lovis, C., Pepe, F., Dumusque, X., . . . Wyttenbach, A. (2016). The HARPS search for southern extra-solar planets—XXXVIII: Bayesian re-analysis of three systems: New super-Earths, unconfirmed signals, and magnetic cycles. *Astronomy & Astrophysics*, 585, A134.
- Doyle, L. R., Carter, J. A., Fabrycky, D. C., Slawson, R. W., Howell, S. B., Winn, J. N., . . . Fischer, D. (2011). Kepler-16: A transiting circumbinary planet. *Science*, 333, 1602.
- Dressing, C. D., & Charbonneau, D. (2015). The occurrence of potentially habitable planets orbiting M dwarfs estimated from the full Kepler dataset and an empirical measurement of the detection sensitivity. *Astrophysical Journal*, 807, 45.
- Dressing, C. D., Charbonneau, D., Dumusque, X., Gettel, S., Pepe, F., Collier Cameron, A., . . . Watson, C. (2015). The mass of Kepler-93b and the composition of terrestrial planets. *Astrophysical Journal*, 800, 135.
- Dumusque, X., Bonomo, A. S., Haywood, R. D., Malavolta, L., Ségransan, D., Buchhave, L. A., . . . Watson, C. (2014). The Kepler-10 planetary system revisited by HARPS-N: A hot rocky world and a solid Neptune-mass planet. *Astrophysical Journal*, 789, 154.
- Dumusque, X., Borsa, F., Damasso, M., Díaz, R. F., Gregory, P. C., Hara, N. C., . . . Udry, S. (2017). Radial-velocity fitting challenge—II. First results of the analysis of the data set. *Astronomy & Astrophysics*, 598, A133.
- Dumusque, X., Pepe, F., Lovis, C., Ségransan, D., Sahlmann, J., Benz, W., . . . Udry, S. (2012). An Earth-mass planet orbiting α Centauri B. *Nature*, 491(7423), 207–211.
- Dumusque, X., Santos, N. C., Udry, S., Lovis, C., & Bonfils, X. (2011a). Planetary detection limits taking into account stellar noise: II. Effect of stellar spot groups on radial-velocities. *Astronomy & Astrophysics*, 527, A82.
- Dumusque, X., Udry, S., Lovis, C., Santos, N. C., & Monteiro, M. J. P. F. G. (2011b). Planetary detection limits taking into account stellar noise: I. Observational strategies to reduce stellar oscillation and granulation effects. *Astronomy & Astrophysics*, 525, A140.
- Einstein, A. (1916). Die Grundlage der allgemeinen Relativitätstheorie. *Annalen der Physik*, 354(7), 769.
- Einstein, A. (1936). Lens-like action of a star by the deviation of light in the gravitational field. *Science*, 84(2188), 506.
- Faria, J. P., Adibekyan, V., Amazo-Gómez, E. M., Barros, S. C. C., Camacho, J. D., Demangeon, O., . . . Viana, P. T. P. (2019). Decoding the radial velocity variations of HD41248 with ESPRESSO. *arXiv e-prints*. arXiv:1911.11714.

- Faria, J. P., Haywood, R. D., Brewer, B. J., Figueira, P., Oshagh, M., Santerne, A., & Santos, N. C. (2016). Uncovering the planets and stellar activity of CoRoT-7 using only radial velocities. *Astronomy & Astrophysics*, 588, A31.
- Faria, J. P., Santos, N. C., Figueira, P., & Brewer, B. J. (2018). Kima: Exoplanet detection in radial velocities. *Journal of Open Source Software*, 3(26), 487.
- Fazio, G. G., Hora, J. L., Allen, L. E., Ashby, M. L. N., Barmby, P., Deutsch, L. K., . . . Cohen, M. (2004). The infrared array camera (IRAC) for the Spitzer space telescope. *Astrophysical Journal Supplement Series*, 154(1), 10–17.
- Feinstein, A. D., Schlieder, J. E., Livingston, J. H., Ciardi, D. R., Howard, A. W., Arnold, L., . . . Treasure, J. (2019). K2-288Bb: A small temperate planet in a low-mass binary system discovered by citizen scientists. *Astronomical Journal*, 157, 40.
- Feroz, F., Balan, S. T., & Hobson, M. P. (2011). Detecting extrasolar planets from stellar radial velocities using Bayesian evidence. *Monthly Notices of the Royal Astronomical Society*, 415(4), 3462–3472.
- Figueira, P., Marmier, M., Bonfils, X., di Folco, E., Udry, S., Santos, N. C., . . . Viana Almeida, P. (2010). Evidence against the young hot-Jupiter around BD +20 1790. *Astronomy & Astrophysics*, 513, L8.
- Figueira, P., Santos, N. C., Pepe, F., Lovis, C., & Nardetto, N. (2013). Line-profile variations in radial-velocity measurements: Two alternative indicators for planetary searches. *Astronomy & Astrophysics*, 557, A93.
- Fischer, D. A., Anglada-Escude, G., Arriagada, P., Baluev, R. V., Bean, J. L., Bouchy, F., . . . Wright, J. T. (2016). State of the field: Extreme precision radial velocities. *Publications of the Astronomical Society of the Pacific*, 128(964), 066001.
- Fischer, D. A., Schwamb, M. E., Schawinski, K., Lintott, C., Brewer, J., Giguere, M., . . . Zimmermann, V. (2012). Planet hunters: The first two planet candidates identified by the public using the Kepler public archive data. *Monthly Notices of the Royal Astronomical Society*, 419, 2900–2911.
- Foo, G., Palacios, D. M., & Swartzlander, G. A. (2005). Optical vortex coronagraph. *Optics Letters*, 30(24), 3308.
- Ford, E. B., Fabrycky, D. C., Steffen, J. H., Carter, J. A., Fressin, F., Holman, M. J., . . . Rowe, J. F. (2012). Transit timing observations from Kepler. II. Confirmation of two multiplanet systems via a non-parametric correlation analysis. *Astrophysical Journal*, 750(2), 113.
- Ford, E. B., & Rasio, F. A. (2008). Origins of eccentric extrasolar planets: Testing the planet-planet scattering model. *Astrophysical Journal*, 686, 621–636.
- Fortney, J. J., Marley, M. S., & Barnes, J. W. (2007). Planetary radii across five orders of magnitude in mass and stellar insolation: Application to transits. *Astrophysical Journal*, 659, 1661–1672.

- Fressin, F., Torres, G., Charbonneau, D., Bryson, S. T., Christiansen, J., Dressing, C. D., . . . Batalha, N. M. (2013). The false positive rate of Kepler and the occurrence of planets. *Astrophysical Journal*, 766, 81.
- Fulton, B. J., Petigura, E. A., Blunt, S., & Sinukoff, E. (2018). RadVel: The radial velocity modeling toolkit. *Publications of the Astronomical Society of the Pacific*, 130(986), 044504.
- Fulton, B. J., Petigura, E. A., Howard, A. W., Isaacson, H., Marcy, G. W., Cargile, P. A., . . . Hirsch, L. A. (2017). The California-Kepler survey. III. A gap in the radius distribution of small planets. *Astrophysical Journal*, 154(3), 109.
- Gaia Collaboration, Brown, A. G. A., Vallenari, A., Prusti, T., de Bruijne, J. H. J., Babusiaux, C., . . . Zwitter, T. (2018). Gaia data release 2. Summary of the contents and survey properties. *Astronomy & Astrophysics*, 616, A1.
- Gardner, J. P., Mather, J. C., Clampin, M., Doyon, R., Greenhouse, M. A., Hammel, H. B., . . . Wright, G. S. (2006). The James Webb space telescope. *Space Science Reviews*, 123(4), 485–606.
- Gaudi, B. S., Bennett, D. P., Udalski, A., Gould, A., Christie, G. W., Maoz, D., . . . Macintosh, B. (2008). Discovery of a Jupiter/Saturn analog with gravitational microlensing. *Science*, 319(5865), 927.
- Giguere, M. J., Fischer, D. A., Zhang, C. X. Y., Matthews, J. M., Cameron, C., & Henry, G. W. (2016). A combined spectroscopic and photometric stellar activity study of Epsilon Eridani. *Astrophysical Journal*, 824(2), 150.
- Gillon, M., Jehin, E., Lederer, S. M., Delrez, L., de Wit, J., Burdanov, A., . . . Queloz, D. (2016). Temperate Earth-sized planets transiting a nearby ultracool dwarf star. *Nature*, 533, 221–224.
- Gillon, M., Jehin, E., Magain, P., Chantry, V., Hutsemékers, D., Manfroid, J., . . . Udry, S. (2011). TRAPPIST: A robotic telescope dedicated to the study of planetary systems. *European Physical Journal Web of Conferences*, 11, 06002.
- Gillon, M., Triaud, A. H. M. J., Demory, B.-O., Jehin, E., Agol, E., Deck, K. M., . . . Queloz, D. (2017). Seven temperate terrestrial planets around the nearby ultracool dwarf star TRAPPIST-1. *Nature*, 542, 456–460.
- Gould, A., & Loeb, A. (1992). Discovering planetary systems through gravitational microlenses. *Astrophysical Journal*, 396, 104–114.
- Grunblatt, S. K., Howard, A. W., & Haywood, R. D. (2015). Determining the mass of Kepler-78b with nonparametric gaussian process estimation. *Astrophysical Journal*, 808(2), 127.
- Guillot, T., Santos, N. C., Pont, F., Iro, N., Melo, C., & Ribas, I. (2006). A correlation between the heavy element content of transiting extrasolar planets and the metallicity of their parent stars. *Astronomy & Astrophysics*, 453(2), L21–L24.
- Guyon, O., Pluzhnik, E. A., Kuchner, M. J., Collins, B., & Ridgway, S. T. (2006). Theoretical limits on extrasolar terrestrial planet detection with coronagraphs. *Astrophysical Journal Supplement Series*, 167(1), 81.

-
- Hara, N. C., Boué, G., Laskar, J., & Correia, A. C. M. (2017). Radial velocity data analysis with compressed sensing techniques. *Monthly Notices of the Royal Astronomical Society*, 464(1), 1220–1246.
- Hatzes, A. P. (2014). The detection of Earth-mass planets around active stars. The mass of Kepler-78b. *Astronomy & Astrophysics*, 568, A84.
- Hatzes, A. P., & Cochran, W. D. (1993). Long-period radial velocity variations in three K giants. *Astrophysical Journal*, 413, 339–348.
- Hatzes, A. P., Dvorak, R., Wuchterl, G., Guterman, P., Hartmann, M., Fridlund, M., . . . Pätzold, M. (2010). An investigation into the radial velocity variations of CoRoT-7. *Astronomy & Astrophysics*, 520, A93.
- Hatzes, A. P., & Rauer, H. (2015). A definition for giant planets based on the mass-density relationship. *Astrophysical Journal*, 810, L25.
- Haywood, R. D., Collier Cameron, A., Queloz, D., Barros, S. C. C., Deleuil, M., Fares, R., . . . Unruh, Y. C. (2014). Planets and stellar activity: Hide and seek in the CoRoT-7 system. *Monthly Notices of the Royal Astronomical Society*, 443, 2517–2531.
- Hébrard, G., Bouchy, F., Pont, F., Loeillet, B., Rabus, M., Bonfils, X., . . . Vidal-Madjar, A. (2008). Misaligned spin-orbit in the XO-3 planetary system? *Astronomy & Astrophysics*, 488(2), 763–770.
- Hecht, E. (2002). *Optics*. New York, NY: Addison Wesley.
- Heng, K., & Showman, A. P. (2015). Atmospheric dynamics of hot exoplanets. *Annual Review of Earth and Planetary Sciences*, 43, 509–540.
- Hilditch, R. W. (2001). *An introduction to close binary stars*. Cambridge, UK: Cambridge University Press.
- Howard, A. W. (2013). Observed properties of extrasolar planets. *Science*, 340(6132), 572–576.
- Howard, A. W., Marcy, G. W., Bryson, S. T., Jenkins, J. M., Rowe, J. F., Batalha, N. M., . . . MacQueen, P. J. (2012). Planet occurrence within 0.25 AU of solar-type stars from Kepler. *The Astrophysical Journal Supplement Series*, 201(2), 15.
- Irwin, J., Charbonneau, D., Nutzman, P., Falco, E., & Stempels, E. (2009). The MEarth project: Searching for transiting habitable super-Earths around nearby M dwarfs. *Proceedings of the International Astronomical Union*, 4(S253), 37–43.
- Jenkins, J. M. (2002). The impact of solar-like variability on the detectability of transiting terrestrial planets. *Astrophysical Journal*, 575, 493–505.
- Jenkins, J. S., & Tuomi, M. (2014). The curious case of HD 41248. A pair of static signals buried behind red noise. *Astrophysical Journal*, 794(2), 110.
- Jontof-Hutter, D., Rowe, J. F., Lissauer, J. J., Fabrycky, D. C., & Ford, E. B. (2015). The mass of the Mars-sized exoplanet Kepler-138 b from transit timing. *Nature*, 522(7556), 321–323.

-
- Jorissen, A., Mayor, M., & Udry, S. (2001). The distribution of exoplanet masses. *Astronomy & Astrophysics*, 379, 992–998.
- Kaltenegger, L., & Sasselov, D. (2011). Exploring the habitable zone for Kepler planetary candidates. *Astrophysical Journal*, 736(2), L25.
- Kasting, J. F., Whitmire, D. P., & Reynolds, R. T. (1993). Habitable zones around main sequence stars. *Icarus*, 101(1), 108–128.
- Kjeldsen, H., Bedding, T. R., Butler, R. P., Christensen-Dalsgaard, J., Kiss, L. L., McCarthy, C., . . . Wright, J. T. (2005). Solar-like oscillations in *α* Centauri B. *Astrophysical Journal*, 635(2), 1281–1290.
- Knutson, H. A., Charbonneau, D., Allen, L. E., Fortney, J. J., Agol, E., Cowan, N. B., . . . Megeath, S. T. (2007). A map of the day-night contrast of the extrasolar planet HD 189733b. *Nature*, 447(7141), 183.
- Koll, D. D. B., Malik, M., Mansfield, M., Kempton, E. M. R., Kite, E., Abbot, D., & Bean, J. L. (2019). Identifying candidate atmospheres on rocky M dwarf planets via eclipse photometry. *Astrophysical Journal*, 886(2), 140.
- Konopacky, Q. M., Barman, T. S., Macintosh, B. A., & Marois, C. (2013). Detection of carbon monoxide and water absorption lines in an exoplanet atmosphere. *Science*, 339(6126), 1398–1401.
- Kopparapu, R. K., Ramirez, R., Kasting, J. F., Eymet, V., Robinson, T. D., Mahadevan, S., . . . Deshpande, R. (2013). Habitable zones around main-sequence stars: New estimates. *Astrophysical Journal*, 765(2), 131.
- Kovács, G., Zucker, S., & Mazeh, T. (2002). A box-fitting algorithm in the search for periodic transits. *Astronomy & Astrophysics*, 391(1), 369–377.
- Kreidberg, L., Koll, D. D. B., Morley, C., Hu, R., Schaefer, L., Deming, D., . . . Vanderspek, R. (2019). Absence of a thick atmosphere on the terrestrial exoplanet LHS 3844b. *Nature*, 573(7772), 87–90.
- Lagrange, A.-M., Bonnefoy, M., Chauvin, G., Apai, D., Ehrenreich, D., Boccaletti, A., . . . Kasper, M. (2010). A giant planet imaged in the disk of the young star β Pictoris. *Science*, 329(5987), 57.
- Lanza, A. F., Malavolta, L., Benatti, S., Desidera, S., Bignamini, A., Bonomo, A. S., . . . Rainer, M. (2018). The GAPS Programme with HARPS-N at TNG—XVII: Line profile indicators and kernel regression as diagnostics of radial-velocity variations due to stellar activity in solar-like stars. *Astronomy & Astrophysics*, 616, A155.
- Latham, D. W., Mazeh, T., Stefanik, R. P., Mayor, M., & Burki, G. (1989). The unseen companion of HD114762: A probable brown dwarf. *Nature*, 339(6219), 38–40.
- Léger, A., Rouan, D., Schneider, J., Barge, P., Fridlund, M., Samuel, B., . . . Zanatta, P. (2009). Transiting exoplanets from the CoRoT space mission. VIII: CoRoT-7b: The first super-Earth with measured radius. *Astronomy & Astrophysics*, 506, 287–302.

-
- Léger, A., Selsis, F., Sotin, C., Guillot, T., Despois, D., Mawet, D., . . . Lammer, H. (2004). A new family of planets? "Ocean-Planets." *Icarus*, 169, 499–504.
- Lendl, M., Delrez, L., Gillon, M., Madhusudhan, N., Jehin, E., Queloz, D., . . . Hellier, C. (2016). FORS2 observes a multi-epoch transmission spectrum of the hot Saturn-mass exoplanet WASP-49b. *Astronomy & Astrophysics*, 587, A67.
- Lindegren, L., Lammers, U., Bastian, U., Hernández, J., Klioner, S., Hobbs, D., . . . O'Mullane, W. (2016). Gaia data release 1: Astrometry: One billion positions, two million proper motions and parallaxes. *Astronomy & Astrophysics*, 595, A4.
- Lissauer, J. J., Fabrycky, D. C., Ford, E. B., Borucki, W. J., Fressin, F., Marcy, G. W., . . . Batalha, N. M. (2011). A closely packed system of low-mass, low-density planets transiting Kepler-11. *Nature*, 470, 53–58.
- Luger, R., Sestovic, M., Kruse, E., Grimm, S. L., Demory, B.-O., Agol, E., . . . Queloz, D. (2017). A seven-planet resonant chain in TRAPPIST-1. *Nature Astronomy*, 1(6), 0129.
- Lyot, B. (1932). Étude de la couronne solaire en dehors des éclipses. Avec 16 figures dans le texte. *Zeitschrift fur Astrophysik*, 5, 73.
- Macintosh, B., Graham, J. R., Barman, T., De Rosa, R. J., Konopacky, Q., Marley, M. S., . . . Zuckerman, B. (2015). Discovery and spectroscopy of the young jovian planet 51 Eri b with the Gemini Planet Imager. *Science*, 350(6256), 64.
- Mahadevan, S., Ramsey, L., Wright, J., Endl, M., Redman, S., Bender, C., . . . Zhao, B. (2010). The habitable zone planet finder: A proposed high-resolution NIR spectrograph for the Hobby Eberly Telescope to discover low-mass exoplanets around M dwarfs. In *Ground-based and Airborne Instrumentation for Astronomy III* (Vol. 7735, p.77356X). Bellingham, WA: International Society for Optics and Photonics.
- Mandel, K., & Agol, E. (2002). Analytic light curves for planetary transit searches. *Astrophysical Journal*, 580, L171–L175.
- Mao, S., & Paczynski, B. (1991). Gravitational microlensing by double stars and planetary systems. *Astrophysical Journal*, 374, L37.
- Marconi, A., Allende Prieto, C., Amado, P. J., Amate, M., Augusto, S. R., Becerril, S., . . . Zackrisson, E. (2018). ELTHIRES, the high resolution spectrograph for the ELT: Results from the Phase A study. In *Ground-based and Airborne Instrumentation for Astronomy VII*, (Vol. 10702, p. 107021Y). Bellingham, WA: Society of Photo-Optical Instrumentation Engineers (SPIE) Conference Series.
- Marcy, G. W., & Butler, R. P. (1996). A planetary companion to 70 Virginis. *Astrophysical Journal*, 464(2), L147.
- Marcy, G. W., Butler, R. P., Vogt, S. S., Fischer, D., & Lissauer, J. J. (1998). A planetary companion to a nearby M4 dwarf, Gliese 876. *Astrophysical Journal Letters*, 505(2), L147.
- Marcy, G. W., Isaacson, H., Howard, A. W., Rowe, J. F., Jenkins, J. M., Bryson, S. T., . . . Barrado, D. (2014). Masses, radii, and orbits of small Kepler planets: The transition from gaseous to rocky planets. *Astrophysical Journal Supplement Series*, 210(2), 20.

-
- Marois, C., Doyon, R., Racine, R., & Nadeau, D. (2000). Efficient speckle noise attenuation in faint companion imaging. *Publications of the Astronomical Society of the Pacific*, 112(767), 91.
- Marois, C., Lafrenière, D., Doyon, R., Macintosh, B., & Nadeau, D. (2006). Angular differential imaging: A powerful high-contrast imaging technique. *The Astrophysical Journal*, 641(1), 556.
- Marois, C., Macintosh, B., Barman, T., Zuckerman, B., Song, I., Patience, J., . . . Doyon, R. (2008). Direct imaging of multiple planets orbiting the star HR 8799. *Science*, 322(5906), 1348.
- Martins, J. H. C., Santos, N. C., Figueira, P., Faria, J. P., Montalto, M., Boisse, I., . . . Cunha, D. (2015). Evidence for a spectroscopic direct detection of reflected light from 51 Pegasi b. *Astronomy & Astrophysics*, 576, A134.
- Mawet, D., Riaud, P., Absil, O., & Surdej, J. (2005). Annular groove phase mask coronagraph. *Astrophysical Journal*, 633(2), 1191.
- Mayor, M., Lovis, C., & Santos, N. C. (2014). Doppler spectroscopy as a path to the detection of Earth-like planets. *Nature*, 513(7518), 328–335.
- Mayor, M., & Queloz, D. (1995). A Jupiter-mass companion to a solar-type star. *Nature*, 378(6555), 355–359.
- McArthur, B. E., Endl, M., Cochran, W. D., Benedict, G. F., Fischer, D. A., Marcy, G. W., . . . Harrison, T. E. (2004). Detection of a Neptune-mass planet in the ρ 1 Cancri system using the Hobby-Eberly telescope. *Astrophysical Journal*, 614(1), L81.
- McCauliff, S. D., Jenkins, J. M., Catanzarite, J., Burke, C. J., Coughlin, J. L., Twicken, J. D., . . . Cote, M. (2015). Automatic classification of Kepler planetary transit candidates. *Astrophysical Journal*, 806, 6.
- Meunier, N., & Lagrange, A. M. (2019). Activity time series of old stars from late F to early K. II. Radial velocity jitter and exoplanet detectability. *Astronomy & Astrophysics*, 628, A125.
- Mordasini, C., Alibert, Y., Benz, W., Klahr, H., & Henning, T. (2012). Extrasolar planet population synthesis: IV. Correlations with disk metallicity, mass, and lifetime. *Astronomy & Astrophysics*, 541, A97.
- Morton, T. D. (2012). An efficient automated validation procedure for exoplanet transit candidates. *Astrophysical Journal*, 761, 6.
- Morton, T. D. (2015). VESPA: False positive probabilities calculator. *Astrophysics Source Code Library*.
- Morton, T. D., & Johnson, J. A. (2011). On the low false positive probabilities of Kepler planet candidates. *Astrophysical Journal*, 738(2), 170.
- Oliva, E., Origlia, L., Maiolino, R., Gennari, S., Biliotti, V., Rossetti, E. . . Sozzi, M. (2004). GIANO: An ultrastable IR echelle spectrometer optimized for high-precision radial velocity measurements and for high-throughput low-resolution spectroscopy. *Proceedings SPIE 5492: Ground-Based Instrumentation for Astronomy*.

Osborn, H. P., Ansdell, M., Ioannou, Y., Sasdelli, M., Angerhausen, D., Caldwell, D. A., . . . Smith, J. C. (2019). Rapid classification of TESS planet candidates with convolutional neural networks. *arXiv e-prints*. arXiv:1902.08544.

Oshagh, M., Boisse, I., Boué, G., Montalto, M., Santos, N. C., Bonfils, X., & Haghighipour, N. (2013a). SOAP-T: A tool to study the light curve and radial velocity of a system with a transiting planet and a rotating spotted star. *Astronomy & Astrophysics*, 549, A35.

Oshagh, M., Santos, N. C., Boisse, I., Boué, G., Montalto, M., Dumusque, X., & Haghighipour, N. (2013b). Effect of stellar spots on high-precision transit light-curve. *Astronomy & Astrophysics*, 556, A19.

Oshagh, M., Santos, N. C., Figueira, P., Barros, S. C. C., Donati, J.-F., Adibekyan, V., . . . Udry, S. (2017). Understanding stellar activity-induced radial velocity jitter using simultaneous K2 photometry and HARPS RV measurements. *Astronomy & Astrophysics*, 606, A107.

Owen, J. E., & Wu, Y. (2017). The evaporation valley in the Kepler planets. *Astrophysical Journal*, 847(1), 29.

Pepe, F., Cameron, A. C., Latham, D. W., Molinari, E., Udry, S., Bonomo, A. S., . . . Watson, C. A. (2013). An Earth-sized planet with an Earth-like density. *Nature*, 503(7476), 377–380.

Pepe, F., Lovis, C., Ségransan, D., Benz, W., Bouchy, F., Dumusque, X., . . . Udry, S. (2011). The HARPS search for Earth-like planets in the habitable zone: I. Very low-mass planets around HD 20794, HD 85512, and HD 192310. *Astronomy & Astrophysics*, 534, A58.

Pepe, F., Molaro, P., Cristiani, S., Rebolo, R., Santos, N. C., Dekker, H., . . . Di Marcantonio, P. (2014). ESPRESSO: The next European exoplanet hunter. *Astronomische Nachrichten*, 335(1), 8–20.

Perryman, M. (2018). *The exoplanet handbook*. Cambridge, UK: Cambridge University Press.

Press, W. H., Teukolsky, S. A., Vetterling, W. T., & Flannery, B. P. (1992). *Numerical recipes in FORTRAN. The art of scientific computing*. Cambridge, U.K.: Cambridge University Press.

Queloz, D., Bouchy, F., Moutou, C., Hatzes, A., Hébrard, G., Alonso, R., . . . Wuchterl, G. (2009). The CoRoT-7 planetary system: Two orbiting super-Earths. *Astronomy & Astrophysics*, 506(1), 303–319.

Queloz, D., Henry, G. W., Sivan, J. P., Baliunas, S. L., Beuzit, J. L., Donahue, R. A., Mayor, M., Naef, D., Perrier, C., and Udry, S. (2001). No planet for HD 166435. *Astronomy & Astrophysics*, 379(1), 279–287.

Queloz, D., Mayor, M., Weber, L., Blécha, A., Burnet, M., Confino, B., . . . Udry, S. (2000). The CORALIE survey for southern extra-solar planets. I. A planet orbiting the star Gliese 86. *Astronomy & Astrophysics*, 354, 99–102.

Quinn, S. N., White, T. R., Latham, D. W., Chaplin, W. J., Handberg, R., Huber, D., . . . Kuszlewicz, J. S. (2015). Kepler-432: A red giant interacting with one of its two long-period giant planets. *Astrophysical Journal*, 803, 49.

- Quirrenbach, A., Amado, P. J., Mandel, H., Caballero, J. A., Mundt, R., Ribas, I., . . . Xu, W. (2010). CARMENES: Calar Alto high-resolution search for M dwarfs with exoEarths with a near-infrared Echelle spectrograph. In Editor(s): I. S. McLean, S. K. Ramsay, & H. Takami (Eds.), *Ground-based and airborne instrumentation for astronomy III* (Vol. 7735, p. 773513). Bellingham, Washington, DC: International Society for Optics and Photonics.
- Racine, R., Walker, G. A. H., Nadeau, D., Doyon, R., & Marois, C. (1999). Speckle noise and the detection of faint companions. *Publications of the Astronomical Society of the Pacific*, 111(759), 587.
- Rajpaul, V., Aigrain, S., & Roberts, S. (2016). Ghost in the time series: No planet for Alpha Cen B. *Monthly Notices of the Royal Astronomical Society: Letters*, 456(1), L6–L10.
- Rajpaul, V., Buchhave, L. A., & Aigrain, S. (2017). Pinning down the mass of Kepler-10c: The importance of sampling and model comparison. *Monthly Notices of the Royal Astronomical Society*, 471(1), L125–L130.
- Rasio, F. A., & Ford, E. B. (1996). Dynamical instabilities and the formation of extrasolar planetary systems. *Science*, 274, 954–956.
- Rauer, H., Catala, C., Aerts, C., Appourchaux, T., Benz, W., Brandeker, A., . . . Zwintz, K. (2014). The PLATO 2.0 mission. *Experimental Astronomy*, 38(1–2), 249–330.
- Ribas, I., Bolmont, E., Selsis, F., Reiners, A., Leconte, J., Raymond, S. N., . . . Anglada-Escudé, G. (2016). The habitability of Proxima Centauri b—I: Irradiation, rotation and volatile inventory from formation to the present. *Astronomy & Astrophysics*, 596, A111.
- Ribas, I., Tuomi, M., Reiners, A., Butler, R. P., Morales, J. C., Perger, M., . . . Anglada-Escudé, G. (2018). A candidate super-Earth planet orbiting near the snow line of Barnard's star. *Nature*, 563(7731), 365.
- Ricker, G. R., Vanderspek, R., Winn, J., Seager, S., Berta-Thompson, Z., Levine, A., . . . Udry, S. (2016). The transiting exoplanet survey satellite <<https://doi.org/10.11117/1.JATIS.1.1.014003>>. *Journal of Astronomical Telescopes, Instruments, and Systems*, 1(1), 014003.
- Robertson, P., & Mahadevan, S. (2014). Disentangling planets and stellar activity for Gliese 667C. *Astrophysical Journal*, 793(2), L24.
- Rogers, L. A. (2015). Most 1.6 Earth-radius planets are not rocky. *Astrophysical Journal*, 801(1), 41.
- Rogers, L. A., Bodenheimer, P., Lissauer, J. J., & Seager, S. (2011). Formation and structure of low-density exo-Neptunes. *Astrophysical Journal*, 738, 59.
- Rouan, D., Riaud, P., Boccaletti, A., Clénet, Y., & Labeyrie, A. (2000). The four-quadrant phase-mask coronagraph. I. Principle. *Publications of the Astronomical Society of the Pacific*, 112(777), 1479.
- Saar, S. H., & Donahue, R. A. (1997). Activity-related radial velocity variation in cool stars. *Astrophysical Journal*, 485(1), 319.

Santerne, A., Brugger, B., Armstrong, D. J., Adibekyan, V., Lillo-Box, J., Gosselin, H., . . . Vigan, A. (2018). An Earth-sized exoplanet with a Mercury-like composition. *Nature Astronomy*, 2, 393–400.

Santerne, A., Fressin, F., Díaz, R. F., Figueira, P., Almenara, J. M., & Santos, N. C. (2013). The contribution of secondary eclipses as astrophysical false positives to exoplanet transit surveys. *Astronomy & Astrophysics*, 557, A139.

Santerne, A., Moutou, C., Tsantaki, M., Bouchy, F., Hébrard, G., Adibekyan, V., . . . Santos, N. C. (2016). SOPHIE velocimetry of Kepler transit candidates—XVII: The physical properties of giant exoplanets within 400 days of period. *Astronomy & Astrophysics*, 587, A64.

Santos, N. C., Bouchy, F., Mayor, M., Pepe, F., Queloz, D., Udry, S., . . . Vauclair, S. (2004). The HARPS survey for southern extra-solar planets—II: A 14 Earth-masses exoplanet around μ Arae. *Astronomy & Astrophysics*, 426(1), L19.

Santos, N. C., & Buchhave, L. A. (2018). Accurate stellar parameters for radial velocity surveys. In H. J. Deeg & J. A. Belmonte (Eds.), *Handbook of exoplanets* (p. 181). Cham, Switzerland: Springer International.

Santos, N. C., Mayor, M., Naef, D., Pepe, F., Queloz, D., Udry, S., . . . Revaz, Y. (2000). The CORALIE survey for Southern extra-solar planets. III. A giant planet in orbit around HD 192263. *Astronomy & Astrophysics*, 356, 599–602.

Santos, N. C., Mortier, A., Faria, J. P., Dumusque, X., Adibekyan, V. Z., Delgado-Mena, E., . . . Udry, S. (2014). The HARPS search for southern extra-solar planets: XXXV. The interesting case of HD 41248: Stellar activity, no planets? *Astronomy & Astrophysics*, 566, A35.

Schanche, N., Collier Cameron, A., Hébrard, G., Nielsen, L., Triaud, A. H. M. J., Almenara, J. M., . . . Wheatley, P. J. (2019). Machine-learning approaches to exoplanet transit detection and candidate validation in wide-field ground-based surveys. *Monthly Notices of the Royal Astronomical Society*, 483, 5534–5547.

Schneider, J., Dedieu, C., Le Sidaner, P., Savalle, R., & Zolotukhin, I. (2011). Defining and cataloging exoplanets: The exoplanet.eu database. *Astronomy & Astrophysics*, 532, A79.

Seager, S., Dotson, R., & Lunar and Planetary Institute (Eds.). (2010). *Exoplanets*. The University of Arizona space science series. In collaboration with Lunar and Planetary Institute. Tucson, AZ: University of Arizona Press.

Seager, S., Kuchner, M., Hier-Majumder, C. A., & Militzer, B. (2007). Mass-radius relationships for solid exoplanets. *Astrophysical Journal*, 669, 1279–1297.

Seager, S., & Mallén-Ornelas, G. (2003). A unique solution of planet and star parameters from an extrasolar planet transit light curve. *The Astrophysical Journal*, 585(2), 1038.

Shallue, C. J., & Vanderburg, A. (2018). Identifying exoplanets with deep learning: A five-planet resonant chain around Kepler-80 and an eighth planet around Kepler-90. *Astrophysical Journal*, 155(2), 94.

- Sing, D. K., Fortney, J. J., Nikolov, N., Wakeford, H. R., Kataria, T., Evans, T. M., . . . Wilson, P. A. (2016). A continuum from clear to cloudy hot-Jupiter exoplanets without primordial water depletion. *Nature*, 529, 59–62.
- Snellen, I., de Kok, R., de Mooij, E., Brogi, M., Nefs, B., & Albrecht, S. (2010a). Exoplanet atmospheres at high spectral resolution: A CRIRES survey of hot-Jupiters. *Proceedings of the International Astronomical Union*, 6(S276), 208–211.
- Snellen, I. A. G., de Kok, R. J., de Mooij, E. J. W., & Albrecht, S. (2010b). The orbital motion, absolute mass, and high-altitude winds of exoplanet HD209458b. *Nature*, 465(7301), 1049–1051.
- Sozzetti, A., Casertano, S., Lattanzi, M. G., & Spagna, A. (2001). Detection and measurement of planetary systems with GAIA. *Astronomy & Astrophysics*, 373(3), L21–L24.
- Stevenson, K. B., Désert, J.-M., Line, M. R., Bean, J. L., Fortney, J. J., Showman, A. P., . . . Homeier, D. (2014). Thermal structure of an exoplanet atmosphere from phase-resolved emission spectroscopy. *Science*, 346(6211), 838.
- Strehl, K. (1902). Über die Bildschärfe der Fernrohre. *Astronomische Nachrichten*, 158(6), 89.
- Thiabaud, A., Marboeuf, U., Alibert, Y., Leya, I., & Mezger, K. (2015). Elemental ratios in stars vs planets. *Astronomy & Astrophysics*, 580, A30.
- Thompson, S. E., Coughlin, J. L., Hoffman, K., Mullally, F., Christiansen, J. L., Burke, C. J., . . . Borucki, W. J. (2018). Planetary candidates observed by Kepler. VIII. A fully automated catalog with measured completeness and reliability based on data release 25. *Astrophysical Journal Supplement Series*, 235(2), 38.
- Tinetti, G., Drossart, P., Eccleston, P., Hartogh, P., Heske, A., Leconte, J., . . . Zapatero-Osorio, M. R. (2016). The science of ARIEL (Atmospheric Remote-sensing Infrared Exoplanet Large-survey). *Proceedings SPIE 9904: Space Telescopes and Instrumentation 2016: Optical, Infrared, and Millimeter Wave*.
- Torres, G., Fressin, F., Batalha, N. M., Borucki, W. J., Brown, T. M., Bryson, S. T., . . . Welsh, W. F. (2011). Modeling Kepler transit light curves as false positives: Rejection of blend scenarios for Kepler-9, and validation of Kepler-9 d, A super-earth-size planet in a multiple system. *Astrophysical Journal*, 727(1), 24.
- Torres, G., Kipping, D. M., Fressin, F., Caldwell, D. A., Twicken, J. D., Ballard, S., . . . Quintana, E. V. (2015). Validation of 12 small Kepler transiting planets in the habitable zone. *Astrophysical Journal*, 800(2), 99.
- Tuomi, M., & Jones, H. R. A. (2012). Probabilities of exoplanet signals from posterior samplings. *Astronomy & Astrophysics*, 544, A116.
- Turbet, M., Leconte, J., Selsis, F., Bolmont, E., Forget, F., Ribas, I., . . . Anglada- Escudé, G. (2016). The habitability of Proxima Centauri b—II: Possible climates and observability. *Astronomy & Astrophysics*, 596, A112.
- Udry, S., & Santos, N. C. (2007). Statistical properties of exoplanets. *Annual Review of Astronomy and Astrophysics*, 45(1), 397–439.

-
- Valencia, D., O'Connell, R. J., & Sasselov, D. (2006). Internal structure of massive terrestrial planets. *Icarus*, 181(2), 545–554.
- van de Kamp, P. (1983). Planetarische Begleiter von Sternen. *Astronomische Nachrichten*, 304(3), 97–100.
- Van Eylen, V., Agentoft, C., Lundkvist, M. S., Kjeldsen, H., Owen, J. E., Fulton, B. J., . . . Snellen, I. (2018). An asteroseismic view of the radius valley: Stripped cores, not born rocky. *Monthly Notices of the Royal Astronomical Society*, 479(4), 4786–4795.
- Weidenschilling, S. J., & Marzari, F. (1996). Gravitational scattering as a possible origin for giant planets at small stellar distances. *Nature*, 384, 619–621.
- Weiss, L. M., Rogers, L. A., Isaacson, H. T., Agol, E., Marcy, G. W., Rowe, J. F., . . . Fabrycky, D. (2016). Revised masses and densities of the planets around Kepler-10. *Astrophysical Journal*, 819(1), 83.
- Wheatley, P. J., Pollacco, D. L., Queloz, D., Rauer, H., Watson, C. A., West, R. G., . . . Neveu, M. (2013). The next generation transit survey (NGTS). *EPJ Web of Conferences*, 47, 13002.
- Wildi, F., Blind, N., Reshetov, V., Hernandez, O., Genolet, L., Conod, U., . . . Saddlemyer, L. (2017). NIRPS: An adaptive-optics assisted radial velocity spectrograph to chase exoplanets around M-stars. *Proceedings SPIE 10400: Techniques and Instrumentation for Detection of Exoplanets VIII*, 1040018.
- Winn, J. N. (2011). *The Rossiter-McLaughlin effect for exoplanets* <<https://doi.org/10.1051/epjconf/20101105002>>. EPJ Web of Conferences, 11, 05002.
- Winn, J. N. (2018). Planet occurrence: Doppler and transit surveys. *arXiv preprint*. arXiv: 1801.08543.
- Winn, J. N., & Fabrycky, D. C. (2015). The occurrence and architecture of exoplanetary systems. *Annual Review of Astronomy and Astrophysics*, 53(1), 409–447.
- Wittenmyer, R. A., Bergmann, C., Horner, J., Clark, J., & Kane, S. R. (2019a). Truly eccentric—II. When can two circular planets mimic a single eccentric orbit? *Monthly Notices of the Royal Astronomical Society*, 484(3), 4230–4238.
- Wittenmyer, R. A., Clark, J. T., Zhao, J., Horner, J., Wang, S., & Johns, D. (2019b). Truly eccentric—I: Revisiting eight single-eccentric planetary systems. *Monthly Notices of the Royal Astronomical Society*, 484(4), 5859–5867.
- Wyttenbach, A., Ehrenreich, D., Lovis, C., Udry, S., & Pepe, F. (2015). Spectrally resolved detection of sodium in the atmosphere of HD189733b with the HARPS spectrograph. *arXiv e-prints*. arXiv:1503.05581 [astroph].
- Zucker, S., & Giryes, R. (2018). Shallow Transits—Deep Learning. I. Feasibility study of deep learning to detect periodic transits of exoplanets. *Astrophysical Journal*, 155, 147.
- Zurlo, A., Vigan, A., Galicher, R., Maire, A.-L., Mesa, D., Gratton, R., . . . Antichi, J. (2016). First light of the VLT planet finder SPHERE. III. New spectrophotometry and astrometry of the HR 8799 exoplanetary system. *Astronomy and Astrophysics*, 587, A57.

Notes

1. Which may not be the case if there are orbital perturbations; the present review does not address that situation; that is discussed in e.g., Correia et al. (2010).
2. This is valid for a generic companion. In this article, in case the companion is a planet, its mass is denoted by M_{pl} .
3. $\sqrt{4/3} = 1.15$ is the median of $1 / \sin i$.
4. For a definition of the habitable zone, see e.g., Kasting, Whitmire, and Reynolds (1993) and Kopparapu et al. (2013).
5. Note that a is related with the orbital period through Kepler's third Law, and thus, with the velocity that the planet has in its orbit, i.e., the velocity at which the planet will cross the stellar disk.
6. Regarding degeneracy in mass-radius relation, a low mass star and a giant planet can have similar radii, and the existence of an extended atmosphere in a low mass planet can completely alter its position in the mass-radius diagram (e.g., Hatzes & Rauer, 2015).
7. The definition of a Super-Earth is not very clear in the literature. However, this review defines it as a planet that has a mass higher than Earth's but a similar composition based on the density derived from its mass and radius.
8. The transit duration of a planet with an orbital period up to 2–3 years is below 1 day.
9. Note that the orbital period of the planet is the same as that of the star.
10. The microlensing method is described in the section “Microlensing”.
11. Multi-planetary systems are now known to be a common phenomenon, see for example the exoplanet catalogues Exoplanet.eu [\(Schneider et al., 2011\)](http://www.exoplanet.eu/) or the NASA Exoplanet Archive [\(NASA Exoplanet Archive\)](https://exoplanetarchive.ipac.caltech.edu/).

Related Articles

Origins of Life: Open Questions and Debates

The Formation and Evolution of the Solar System

Exoplanets: Atmospheres of Hot Jupiters

Planet Formation

Accretion Processes